First posted online on 11 January 2021 as 10.1242/dmm.047738
Access the most recent version at http://dmm.biologists.org/lookup/doi/10.1242/dmm.047738

Neural crest-specific deletion of *Bmp7* leads to midfacial hypoplasia, nasal airway obstruction, and disordered breathing modelling Obstructive Sleep Apnea

Pranidhi Baddam[1], Vivian Biancardi[2*], Daniela M Roth[1*], Farah Eaton[1], Claudine Thereza-Bussolaro[1,3], Rupasri Mandal[4], David S Wishart[4], Amy Barr[5], Joanna MacLean[6,7], Carlos Flores-Mir[1], Silvia Pagliardini[2], Daniel Graf[1,8 #]

Affiliations:

1: School of Dentistry, Faculty of Medicine and Dentistry, University of Alberta, Edmonton, AB, Canada

2: Department of Physiology, Faculty of Medicine and Dentistry, University of Alberta, Edmonton, AB, Canada

3: Department of Dentistry, Hospital dos Pinheiros, UNIFASIPE, Sinop, Mato Grosso, Brazil

4: The Metabolomics Innovation Centre, Department of Biological Sciences, Faculty of Science, University of Alberta, Edmonton, AB, Canada

5: Department of Pharmacology, Faculty of Medicine and Dentistry, University of Alberta, Edmonton, AB, Canada

6: Department of Pediatrics and the Women & Children's Health Research Institute, Faculty of Medicine and Dentistry, University of Alberta

7: Stollery Children's Hospital; Edmonton, AB, Canada

8: Department of Medical Genetics, Faculty of Medicine and Dentistry, University of Alberta, Edmonton, AB, Canada

* Equal contributions

[#] Corresponding Author

Daniel Graf, PhD

Associate Professor

Alberta Dental Association & College Chair for Oral Health Research

School of Dentistry, Faculty of Medicine and Dentistry, University of Alberta

7020N Katz Group Centre for Pharmacy & Health Research

11361-87 Avenue

Edmonton, Alberta, Canada, T6G 2E1

Phone: +1 780 492 4921

E-mail address: dgraf@ualberta.ca

ORCID: 0000-0003-1163-8117

Authors contact information

PB: pranidhi@ualberta.ca

DMR: dmroth@ualberta.ca

VB: biancard@ualberta.ca

FE: featon@ualberta.ca

CTB: bussolar@ualberta.ca

RM: rmandal@ualberta.ca

DSW: dwishart@ualberta.ca

AB: abarr@ualberta.ca

JM: joanna.maclean@ualberta.ca

CFM: cf1@ualberta.ca

SP: silviap@ualberta.ca

DG: dgraf@ualberta.ca

Summary statement

Bmp7 neural crest knockout mouse is a novel model for nasal airway obstruction with a craniofacial origin that allows to study disordered breathing and associated consequences in a physiological context.

Key words: Bone Morphogenetic Protein 7, midfacial hypoplasia, airway obstruction, nasal septum deviation, turbinate hypertrophy, apneas, sleep related breathing disorders.

Abstract

Pediatric obstructive sleep apnea (OSA), a relatively common sleep-related breathing disorder (SRBD) affecting approximately 1-5% of children, is often caused by anatomical obstruction and/or collapse of the nasal and/or pharyngeal airways. The resulting sleep disruption and intermittent hypoxia lead to various systemic morbidities. Predicting the development of OSA from craniofacial features alone is currently not possible and a controversy remains if upper airway obstruction facilitates reduced midfacial growth or vice-versa. Currently, there is no rodent model that recapitulates both the development of craniofacial abnormalities and upper airway obstruction to address these questions. Here, we describe that mice with a neural crest-specific deletion of *Bmp7* (Bmp7^{ncko}) present with shorter, more acute angled cranial base, midfacial hypoplasia, nasal septum deviation, turbinate swelling and branching defects, and nasal airway obstruction. Interestingly, several of these craniofacial features develop after birth during periods of rapid midfacial growth and precede the development of an upper airway obstruction. We identified that in this rodent model, no single feature appeared to predict upper airway obstruction, but the sum of those features resulted in a reduced breathing frequency, apneas and overall reduced oxygen consumption. Metabolomics analysis of serum from peripheral blood identified increased levels of hydroxyproline, a metabolite upregulated under hypoxic conditions. As this model recapitulates many features observed in OSA, it offers unique opportunities for studying how upper airway obstruction affects breathing physiology and leads to systemic morbidities.

Introduction

Sleep related breathing disorders (SRBD) encompasses a spectrum of problems including obstructive sleep apnea (OSA), central sleep apnea (CSA) and complex sleep apnea (Gipson et al., 2019; Morgenthaler et al., 2006). In children, pediatric OSA is the most common and widely investigated form of apnea with a prevalence of 1.2% – 5.7% (Gipson et al., 2019). It is often caused by physical obstruction of either nasal and/or pharyngeal airways leading to reduced airflow intake and/or intermittent apneas resulting in difficulty to breathe. This can lead to intermittent hypoxia conditions most prominently noticed during sleep and has been associated with a variety of systemic morbidities including cardiovascular, metabolic, neurocognitive as well as behavioral problems at home and school that may continue and progress into adulthood (Gozal, 1998; Leger et al., 2012).

The etiology of pediatric OSA is multifactorial. Craniofacial and neuromuscular factors along with lymphoid tissue hypertrophy and airway soft tissue inflammation are considered critical components contributing to pediatric OSA (Bozzini and Di Francesco, 2016); however, controversy remains on cause or consequence of these various manifestations. The resulting intermittent hypoxia is considered a critical factor in the systemic pathogenesis of OSA (Dewan et al., 2015). The gold standard for diagnosis of OSA should include nocturnal polysomnography (nPSG). Chronic untreated OSA can result in cardiovascular, neurocognitive and metabolic morbidities (Gabryelska et al., 2018), whereby the presence of intermittent hypoxia is associated with increased severity of these morbidities (Veasey, 2009). Current surgical approaches are primarily aimed at relieving the physical obstruction (Hoeve et al., 1999). Hypertrophy of tonsils and adenoids can contribute to pharyngeal obstruction. Hence, a common paediatric surgical approach is tonsillectomy and adenoidectomy (T&A) to remove enlarged lymphoid tissue (Carithers et al., 1987). However, upper airway obstruction commonly remains as a post-operative symptom, residual pediatric OSA, suggestive of a more complex, multifactorial aetiology of pediatric OSA/SRBD. The lack of complete resolution with these interventions

also highlights the need to consider various craniofacial components in addition to adenoids (Carithers et al., 1987) for better screening, diagnosis and management outcomes.

Craniofacial abnormalities strongly predispose to upper airway obstruction, as the prevalence of OSA increases to up to 67% in children with craniofacial syndromes (Skotko et al., 2017; Tan et al., 2016). Midfacial hypoplasia, nasal septum deviation, micrognathia, craniosynostosis, achondroplasia and cleft palate are all considered contributing factors to upper airway obstruction (Cielo et al., 2016). A common denominator in all these abnormalities is altered or lack of craniofacial growth. However, it remains unclear if altered growth predisposes to physical upper airway obstruction or vice-versa, since most clinical studies are static retrospective rather than long-term prospective (Cielo et al., 2016).

Various animal models have been used to assess short and long term consequences of SRBD, ranging from experimentally induced hypoxia through the use of hypoxia chambers, forced sleep deprivation, or naturally occurring obstruction models like that of the English Bulldog (Hendricks et al., 1987). Risk factors for SRBD like obesity were also examined (Brennick et al., 2009; Polotsky et al., 2012; Strohl and Thomas, 2001). Whole-body plethysmography was used to assess changes to respiration in rodent models (Chopra et al., 2016). However, none of those models was able to clearly delineate causes and consequences of pediatric OSA. As a result, it remains uncertain whether craniofacial abnormalities such as midfacial hypoplasia precede nasal airway obstruction or whether airway obstruction predisposes or enhances craniofacial abnormalities.

Pierre Robin sequence (PRS) is frequently associated with craniofacial abnormalities such as micrognathia, midfacial hypoplasia, and airway obstruction (Gangopadhyay et al., 2012). Deletion of Bone Morphogenetic Protein 7 (*Bmp7*) in mice recapitulates many of those craniofacial features (Kouskoura et al., 2016). However, complete loss of *Bmp7* results in cleft palate and perinatal lethality (Kouskoura et al., 2013) precluding post-natal assessment of craniofacial growth. Mice with neural crest-

specific deletion of *Bmp7* (Bmp7^{ncko}) survive postnatally and present with micrognathia and midfacial hypoplasia (Kouskoura et al., 2016).

Using micro-computed tomography (μCT) and morphometrics we describe here the sequence of when these midfacial abnormalities develop in Bmp7^{ncko} mice. Unrestrained whole-body plethysmography was used to characterize respiratory function under normoxic, hypoxic and hyperoxic conditions. Oxygen consumption and respiratory gas exchange were monitored using Comprehensive Lab Monitoring System (CLAMS). An unbiased metabolomics analysis on blood serum was conducted to identify changes to metabolites at the onset of upper airway obstruction. We demonstrate a combination of craniofacial defects leads to nasal airway obstruction, and that craniofacial growth deficiencies precede nasal airway obstruction.

To our knowledge, this is the first genetic rodent model of midfacial hypoplasia in which airway obstruction has been assessed. It thus presents as an important model to study etiology and systemic consequences of midfacial hypoplasia. Findings from this study will serve as a foundation to better understand the development and management of pediatric airway obstruction in humans.

Results

Loss of Bmp7 leads to midfacial hypoplasia and early lethality.

Bmp7^{ncko} mice appear inconspicuous during the first two weeks of life. From around 2 weeks of age, a midfacial depression can be observed in the mutants to a varying degree (Figure 1A, B). Starting at about 3 weeks of age, a failure to thrive with variable onset was observed that ultimately led to death, with only 30% of mutant mice surviving past 8 weeks (Figure 1C). To determine if the midfacial depression/hypoplasia is associated with the mortality, a morphometric assessment of the craniofacial complex was conducted on 2-week (P14), 3-week (P21) and 4-week (P30) mice using a landmark-based approach (Wei et al., 2017). A detailed description of the landmarks used can be found in Fig. S1. The difference in facial length (Figure 1F) between Bmp7^{ncko} and control

mice only became significant at P21 (Figure 1D) (p=2.40E-04) as consequence of reduced facial growth between the 2- and 3-week time-points. Although craniofacial growth catches up subsequently, the difference still persisted at P30 (p=2.10E-03). Other craniofacial characteristics like snout angle (Figure 1E, F) frontal bossing (Figure 1G, I), nasal depression (Figure 1H, I), nasal width (Figure 1J, L) and length (Figure 1K, L) showed no significant differences in this limited cohort of mice. The p values for these measurements are provided in Table S1. This morphometric analysis establishes that deletion of *Bmp7* from neural crest cells leads to midfacial hypoplasia that becomes prominent around P21.

$Bmp7^{ncko}$ develop craniofacial abnormalities commonly observed in children with midfacial hypoplasia

We next performed a detailed morphometric analysis on a larger cohort of 4-week old $Bmp7^{ctrl}$ and $Bmp7^{ncko}$ mice to test for additional craniofacial alterations commonly observed in children with midfacial hypoplasia and upper airway obstruction (Cielo et al., 2016). Landmark-based morphometrics (for details see Fig. S1) identified a more acutely angled cranial base (p=1.7E-02; Figure 2A-B) with a significantly shorter basisphenoid (BS) (p=3.58E-06; Figure 2C-D). No significant changes were observed in the length of the basioccipital, presphenoid and ethmoid bones (Table S2). Assessment at earlier time-points (P14, P21) showed no significant changes (Table S3). Significant length reductions were found both for the posterior (p=2.44E-05) and anterior frontal complex (p=1.18E-06; Figure 2E-F). Changes to snout angle (Figure 2G-H), frontal bossing angle (Figure 2G-H), nasal depression angle (Figure 2G-H) along with nasal width (Figure 2I-J) and length (Figure 2I-J) are a reflection of the significantly more acute angled snout (p=1.43E-05), depressed nasal bones (p=3.21E-07), and increased frontal bossing (p=4.84E-06) in 1-month old $Bmp7^{ncko}$ mice. Additionally, the length (p=3.80E-03) but not width of the nasal bones was significantly reduced. Overall, these findings are consistent with features of midfacial hypoplasia and reduced upper airway space.

In addition to changes to cranial base length and angle, two other craniofacial differences are commonly observed in children with midfacial hypoplasia and upper airway obstruction: nasal septum deviation and turbinate hypertrophy (Milanesi et al., 2019). To characterize potential changes to nasal septum and turbinates, frontal (blue line, Figure 3) and axial planes (orange line, Figure 3) were identified from µCT scans of P14 and P30 mice skulls. The nasal septum (pink arrows, Figure 3) in P14 $Bmp7^{ctrl}$ (Figure 3A-C) and $Bmp7^{ncko}$ mice (Figure 3D-F) showed no obvious differences on both frontal and axial planes. However, $Bmp7^{ncko}$ mice showed reduced turbinate branching (yellow arrows) and their turbinates appeared larger (Figure 3F). At P30, all $Bmp7^{ncko}$ mice had developed nasal septum deviation (pink arrows) (Figure 3J-O) when compared to controls (Figure 3G-I). The extent, shape, direction and location, as well as the degree of deviation was variable (Figure 3K, N). Turbinate development appeared disturbed. Reduced branching and ossification as well as slight swelling of turbinate soft tissue were apparent bilaterally at P14. This swelling and reduced turbinate branching was even more noticeable at P30 (Figure 3I, L, O). Both nasal septum deviation and turbinate swelling can impede airflow in the nasal cavity thus potentially exacerbating any other physical airway obstruction.

Evidence of spontaneous apneas (SA) and post sigh apneas (PSA) in $Bmp7^{ncko}$ mice

Whole-body plethysmography was used to assess breathing patterns in $Bmp7^{ncko}$ mice. Eight control and ten $Bmp7^{ncko}$ mice were measured at a time when the mutant mice had developed nasal septum deviation (4-6 weeks of age). From the ten $Bmp7^{ncko}$ mice analyzed in this study, five elicited greater spontaneous apneas (SA) in normoxia compared to $Bmp7^{ctrl}$ mice ($p = 4.00E-03$) and the remaining $Bmp7^{ncko\,(r)}$ mice ($p = 2.00E-02$; Figure 4A,B). Consequently, we divided the mutant mice cohort into two groups for all respiratory analysis: $Bmp7^{ncko\,(r)}$ (regular breathing) and $Bmp7^{ncko\,(a)}$ (high frequency SA).

Movie S1 shows recordings of plethysmography traces associated with behaviour of a $Bmp7^{ctrl}$ mouse during eupneic breathing, and $Bmp7^{ncko\,(a)}$ mouse experiencing SA. The presence of greater SA in the $Bmp7^{ncko\,(a)}$ persisted during hypoxia in comparison to

$Bmp7^{ctrl}$ (p = 0.01) as well as during the first minute of recovery to normoxia (p = 5.00E-03; $Bmp7^{ctrl}$: 0.3±0.5; $Bmp7^{ncko\ (r)}$: 3.0±4.7; $Bmp7^{ncko\ (a)}$: 8.2±5.5) (not shown). The presence of greater SA in the $Bmp7^{ncko\ (a)}$ group disappeared during hyperoxia (40% O_2) in comparison to $Bmp7^{ctrl}$ and $Bmp7^{ncko\ (r)}$ groups (p = 0.21 and p = 0.54, respectively; Figure 4B). However, there is one animal that appears to be an outlier, so it was excluded from the statistical analysis for all the gas exposures. These results indicate that during normoxic and hypoxic conditions apneas are more frequent in a subpopulation of $Bmp7^{ncko}$ mice and this difference was eliminated in hyperoxia.

Sigh frequency was comparable between all experimental groups. As expected (Li et al., 2016), hypoxia exposure induced an increased number of sighs in all groups (p < 0.001) compared to normoxia (Figure 4C). Under physiological conditions sighs may be followed by brief apneas (post-sigh apneas - PSA) or respiratory irregularities (Bastianini et al., 2019). Short respiratory disruptions following a sigh (≤ 1 apnea) was reduced in the $Bmp7^{ncko\ (a)}$ group compared to $Bmp7^{ctrl}$ and $Bmp7^{ncko\ (r)}$ (p < 0.01; Figure 4D), whereas prolonged PSA events (≥2 apneas following a sigh, as shown in Fig4A) increased (p < 0.001; Figure 4E).

$Bmp7^{ncko}$ mice with apneas show altered baseline respiratory, metabolic, and thermoregulatory patterns

Along with greater number of SA and longer PSA events, $Bmp7^{ncko\ (a)}$ mice had a lower baseline respiratory frequency (fR) (p =1.60E-02; Figure 5A) and an increase in cycle duration of each respiratory event (T_{TOT}) (p = 4.10E-02) due to an increase in the inspiratory time (T_i; p = 1.90E-02) with a trend to increase the expiratory time (T_e; p = 7.90E-02; Figure 5B). Noteworthy, the two $Bmp7^{ncko\ (a)}$ mice with greater SA number showed greater T_{TOT}, T_i and T_e compared to the other mice from the same group. $Bmp7^{ncko\ (r)}$ mice showed a trend towards reduced values for fR compared to control mice, however, the differences were not significant. Despite fR changes, baseline tidal volume (V_T) and minute ventilation ($\dot{V}_E$) did not differ between the groups (Figure 5C and D, respectively).

Despite the greater number of SA in the $Bmp7^{ncko\ (a)}$ mice, we did not find changes in variability of respiratory parameters among the groups (data not shown) or normoxic O_2 consumption ($\dot{V}O_2$) and air convection requirements ($\dot{V}_E/\dot{V}O_2$) (Figure 5E and F). Overall baseline body temperature (Tb) was lower in the $Bmp7^{ncko\ (r)}$ mice compared to control group (p = 1.20E-02; Figure 5G), mainly due to a greater Tb individual variability within the $Bmp7^{ncko\ (r)}$ mice.

To establish the timeline of when $Bmp7^{ncko}$ mice develop respiratory disturbances, a separate plethysmography assessment was conducted at 2 weeks of age, prior to the development of nasal abnormalities. At this time, the number of SA and PSA were comparable between $Bmp7^{ncko}$ and $Bmp7^{ctrl}$ mice (Fig. S2). However, the $Bmp7^{ncko}$ mice demonstrate a trend towards lower baseline respiratory frequency (fR) and an increase in duration of each respiratory event (T_{TOT}) as a result of an increase in inspiratory (T_i) and expiratory times (T_e). These results suggest that the majority of respiratory disturbances develop following the development of craniofacial abnormalities.

Ventilatory and metabolic responses to hypoxia (10% O_2) and hyperoxia (40% O_2)

The same mice used for breathing analysis in normoxia were exposed to acute hypoxia (10% O_2) and hyperoxia (40% O_2) to evaluate their respiratory responses to different levels of oxygen. In the control group, we observed the biphasic ventilatory response, where hypoxia induced hyperventilation as shown by an increase in $\dot{V}_E$ and $\dot{V}_E/\dot{V}O_2$ in the first 5 min of exposure (p<0.001; Figure 5D and 5F, respectively) followed by an attenuation at 15 min with no significant difference from baseline values. Significant increase in fR was observed both at 5 min (p < 0.001) and at 15 min (p < 0.001; Figure 5A; Fig. S2). Hypoxia also caused a decrease in $\dot{V}O_2$ (p<0.05; Figure 5E) and body temperature (p<0.001; Figure 5G). A comparable physiological response to hypoxia was observed in both $Bmp7^{ncko\ (a)}$ and $Bmp7^{ncko\ (r)}$ groups (p<0.05). Even though $Bmp7^{ncko(a)}$ had a lower breathing frequency in normoxic conditions, the hypoxic frequency response shown as % of baseline was similar among the 3 groups (Fig. S3). However, mice from the $Bmp7^{ncko(r)}$

group showed a variable hypoxic ventilatory response. Two mice showed hyperventilation as seen by larger values in the $\dot{V}_E/\dot{V}O_2$ data (Figure 5F), while the other 3 mice showed no change in $\dot{V}_E/\dot{V}O_2$ compared to normoxia. It is noteworthy that the one Bmp7^{ncko} mouse in which $\dot{V}O_2$ did not drop during hypoxia showed a baseline body temperature of 33°C, which is below the normal range, and no further decrease during hypoxia was observed. Therefore, it is legitimate to deduct that thermoregulation in this specific mouse seemed compromised, potentially further affecting ventilation and O_2 consumption modulation. Interestingly, all Bmp7$^{ncko\ (r)}$ mice showed an increased fR induced by hypoxia at 5 min that persisted throughout the hypoxic exposure ($p<0.01$) (Figure 5A), although no changes were observed for the other physiological variables ($\dot{V}_E$, V_T, $\dot{V}O_2$ and $\dot{V}_E/\dot{V}O_2$).

Hyperoxia did not evoke any changes in the respiratory, metabolic or thermoregulatory variables within and between experimental groups, with the exception of a lower respiratory frequency in Bmp7$^{ncko\ (a)}$ mice during 40% O_2 ($p=5.00E-03$), due to the lower baseline fR.

Reduced delta oxygen and upregulation of hydroxyproline observed in Bmp7^{ncko} mice.

Four-week-old Bmp7^{ctrl} and Bmp7^{ncko} (n=5/genotype) mice were placed individually in CLAMS chambers for 24 hours to measure oxygen consumption and respiratory exchange. Delta oxygen, the difference in oxygen fraction in the inflow and outflow of the chamber, was reduced in Bmp7^{ncko} mice, as shown by representative traces of one control and two Bmp7^{ncko} mice (Figure 6A). The trace of the respiratory exchange ratio (RER), which is the rate of carbon dioxide production to the rate of oxygen consumption, showed no clear differences (Figure 6B). Quantification of ΔO_2 (Figure 6C) and RER (Figure 6D) demonstrated a significant reduction in ΔO_2 ($p<0.05$) and no change to RER in the Bmp7^{ncko} mice. To understand systemic consequences, blood serum from P30 Bmp7^{ctrl} and Bmp7^{ncko} mice (n=5/genotype) was collected and screened for changes to metabolite concentrations using an unbiased metabolomics assay. 154 metabolites were detected and quantified in each sample. A significant upregulation of hydroxyproline

($p<0.05$), an indicator of collagen synthesis or release, was identified in Bmp7^{ncko} mice (Figure 6E). This demonstrated Bmp7^{ncko} mice consume less oxygen over time and it is possible to identify metabolite differences between control and mutant mice.

Bmp7^{ncko} mice show decreased exercise capacity at P30

To test whether Bmp7^{ncko} mice develop reduced endurance for physical activity, mice were assessed on a treadmill longitudinally started at the age of 3 weeks. Physical activity in the mice at 3 weeks was comparable between the groups with an increasing reduction in activity after every subsequent assessment (Figure 6F). The difference in physical ability was confirmed in an acute speed test where Bmp7 mutant mice tired very quickly, spent more time on the resting plate, indicating that they do not have the same capacity for physical exercise (Movie S2). Thus, craniofacial defects and associated breathing disturbances might lead to a reduced ability for physical activity possibly due to airway obstruction in this rodent model.

Discussion

In this study, Bmp7^{ncko} mice revealed structural and growth abnormalities in the craniofacial complex, alteration in breathing pattern, i.e. apnea events and lower breathing frequency, and reduction in the capacity for physical exercise. Thus, the Bmp7^{ncko} mouse model emulates several features often linked to the onset of airway obstruction in pediatric OSA (Cielo et al., 2016), including midfacial hypoplasia, shorter cranial base, and nasal septum deviation. By delineating the sequence of craniofacial changes, we show that they tend to precede the onset of respiratory disturbances. We also show how this model might be used to identify systemic manifestations caused by upper airway obstruction.

Despite the abundance of genetic rodent models of midfacial abnormalities, to our knowledge no rodent model of nasal airway obstruction, SRBD and midfacial deficiency has been described. Such a model could greatly benefit the field of pediatric sleep

medicine. Most rodent models of SRBD and/or airway obstruction address only isolated facets of this complex disorder (Table 1). Animals exhibiting intermittent hypoxia (IH) have most commonly been used to study the effects of obstruction (Fletcher et al., 1992; Gozal et al., 2001). However, there is controversy in whether the settings used to mimic IH in rodent experiments are clinically translatable to IH experienced in humans (Farré et al., 2018). Mechanical obstruction of the airways or oxygen deprivation have also been used (Almendros et al., 2011; Tarasiuk and Segev, 2018). The SRBD/OSA rodent models with "naturally occurring" airway obstruction, such as the Zucker hooded rat (Iida et al., 1996), exhibit loss of airway patency due to excessive soft tissue or obesity. Understanding how abnormalities of the craniofacial complex lead to airway obstruction and SRBD has been hampered by the fact that models with severe congenital craniofacial anomalies, which often involves a cleft palate, die at birth preventing postnatal analysis (Hong and Krauss, 2012; Perlyn et al., 2006). On the other hand, models that show snout asymmetries, as for instance often observed in Bmp7 haploinsufficient mice, have not been assessed for breathing abnormalities or show early lethality as a consequence, thus making the $Bmp7^{ncko}$ model unique. It is the first model to describe how craniofacial abnormalities such as midfacial hypoplasia, short and acute-angled cranial base, and nasal septum deviation predispose mice to nasal airway obstruction postnatally. A shorter cranial base is often associated with premature fusion of cranial base synchondrosis (Rosenberg et al., 1997). Careful examination revealed that this was not the case in $Bmp7^{ncko}$ mice. It is therefore possible that the shorter cranial base is a consequence of reduced growth itself. $Bmp7^{ncko}$ mice develop midfacial hypoplasia during the time of rapid midfacial growth (2-3 weeks of age). Midfacial hypoplasia on its own appears to be insufficient to induce upper airway obstruction. Hypoplasia and associated shorter and more acute angled cranial base and reduced nasal bone length (Figure 1 and 2) are all established prior to nasal airway obstruction. Only once nasal septum deviation and turbinate swelling are observed around 4 weeks, the animals start developing respiratory disturbances. The hypopneas (lower fR), an increase in T_{TOT}, T_i, increased number of SA and PSA irregularities in a

subpopulation of the Bmp7^{ncko} mice are features likely associated with nasal airway obstruction due to the combination of craniofacial abnormalities. Little was known about the sequence, etiology, and consequences of these different craniofacial anomalies. Craniofacial characteristics have been described in detail for several mouse strains with midfacial hypoplasia (Eimar et al., 2016; Marulanda et al., 2017; Suzuki et al., 2016), see also Table 1. None of these models show nasal septum deviation and or nasal airway obstruction, supporting the notion that midfacial hypoplasia on its own does not necessarily lead to nasal airway obstruction (Finkelstein et al., 2000; Tan et al., 2016). The survival plot (Fig. 1C) indicates that the majority of Bmp7^{ncko} mice die by the age of 8-12 weeks, which coincides with plateauing of craniofacial growth (Vora et al., 2015). Although challenging to assess in detail, we believe that cumulative craniofacial changes either fatally affect mice by that age, or will never be sufficiently severe allowing mice to survive long-term.

Similarly, when comparing pediatric OSA cohorts of different ethnicities, differences in the prevalence of craniofacial abnormalities were noted (Lee et al., 2010; Tan et al., 2016). Those ethnicities have distinct craniofacial features with different degrees of sagittal, vertical and transversal maxilla-mandibular interrelations. It was also observed that nasal septum deviation, turbinate hypertrophy and enlarged adenoids greatly increase the prevalence of upper airway obstruction in children with midfacial hypoplasia (Clark et al., 2018; Pacheco et al., 2015; Tan et al., 2016). Turbinate hypertrophy and deviated nasal septum frequently occur together (Baddam et al., 2020; Hsu and Suh, 2018), but again their presence on their own is insufficient to predict upper airway obstruction (Baddam et al., 2020). In Bmp7^{ncko} mice turbinate swelling precedes nasal septum deviation. Currently, the cause of turbinate swelling is unclear. Although abnormal turbinate development can be observed, the swelling could also be a consequence of abnormal mucus drainage, cellular changes to turbinates mucosa and/or altered airflow.

Although all Bmp7^{ncko} develop nasal septum deviation at 4 weeks, 50% of these mice developed SA between 4 and 6 weeks. This is suggestive that Bmp7^{ncko} mice experience respiratory distress due to airway obstruction to varying degrees. Here, we showed evidence that morphological changes in the upper airways disrupt regular breathing pattern possibly due to airway obstruction. An increased inspiratory airway resistance may lead to two mechanisms to maintain ventilation: (1) an increase in inspiratory muscle drive; and (2) an increase in the inspiratory time, to achieve a comparable V_T over an expanded inspiratory time(Hernandez et al., 2012; Mann et al., 2017). In the present study, Bmp7$^{ncko\ (a)}$ mice showed an increased in T_{TOT}, mainly due to an increase in the T_i and a tendency for a prolonged T_e compared to control mice resulting in no changes in V_T and $\dot{V}_E$. In patients with OSA, when these adjustments in breath timing do not compensate ventilation, apneas or hypopneas may occur (Gleadhill et al., 1991; Sanders and Moore, 1983; Yamauchi et al., 2011) as we have observed in a subpopulation of Bmp7^{ncko} mice. Indeed, adaptation to mouth breathing has been observed in children with upper airway obstruction (Trosman and Trosman, 2017). Although mice are described as obligate nose breathers (Harkema and Morgan, 1996), adaptation to mouth breathing (Agrawal et al., 2008; Niaki et al., 2008) or gasping (Khurana and Thach, 1996) has been observed in the event of nasal obstruction. Assuming that adaptation occurs in Bmp7^{ncko} mice, further experiments will be necessary to distinguish adaptation to mechanical and/or central control of breathing.

Along with a greater SA incidence, Bmp7$^{ncko\ (a)}$ mice present also with a greater frequency of irregular breathing following a sigh. The mechanisms underlying apneas and, particularly, PSA are not completely understood. They may involve inhibition of inspiration through activation of pulmonary stretch receptors, the Breuer-Hering reflex, or decreased drive to breathe due to lower CO_2 levels induced by the sigh (Bastianini et al., 2019; Davis and O'Donnell, 2013; Saito et al., 2002). Bmp7$^{ncko\ (a)}$ mice may have alteration in the vagal reflex, or compromised central responses to the reflex, leading to more apneic events, and that could also explain the lower breathing frequency. Derivatives of neural crest

contribute to the carotid body and sensory neurons (Annese et al., 2017; Pavan and Raible, 2012), both of which provide important excitatory signals for central breathing control, especially in hypoxic conditions. Bmp7 could affect the development of either structure. While a role for Bmp7 in neurogenesis is well established (Choe et al., 2013; Segklia et al., 2012) and $Bmp7^{ncko}$ mice show sensory deficits in a van Frey assay (unpublished data), nothing is known about neural crest-derived Bmp7 contribution to carotid body development and function. It should be noted that the Wnt1-Cre driver used in this study has been shown to affect brain development (Lewis et al., 2013). For this reason, Bmp7fx/+;Wnt1Cre mice were additionally assessed for craniofacial changes. There was no evident septum deviation or early lethality as seen in $Bmp7^{ncko}$ mice. Therefore, these mice were not subjected to functional plethysmography.

In the present study, both $Bmp7^{ctrl}$ and $Bmp7^{ncko}$ mice showed a biphasic ventilatory response to hypoxia (Moss, 2000; Teppema and Dahan, 2010), with a decrease in $\dot{V}O_2$ and body temperature (Peña and Ramirez, 2005), indicating that peripheral chemosensitivity and centrally regulated breathing control are most likely intact. However, the drop in Tb was greater in the $Bmp7^{ncko\,(a)}$ mice compared to controls, suggesting that the thermoregulatory control to hypoxia may be affected by deletion of Bmp7 in neural crest.

Supplemental oxygen therapy has been examined to have effects on the pathophysiology of OSA, in humans, although its benefits are controversial (Mehta et al., 2013; Wellman et al., 2008; Xie et al., 2013). We wanted to test if reducing the ventilatory drive with hyperoxia exposure, $Bmp7^{ncko\,(a)}$ mice would show changes in breathing pattern or irregularities. Hyperoxia did not affect the number of PSA, either caused any dysfunction in ventilation. However, it reduced the number of SA in the $Bmp7^{ncko\,(a)}$, except for one mouse in which hyperoxia potentiated the number of SA. These results suggest that, at least in our mouse model, hyperoxia may help reducing the occurrence of SA in $Bmp7^{ncko\,(a)}$ mice. However, the fact that one outlier $Bmp7^{ncko\,(a)}$ mouse showed the opposite effect should not be ignored. The respiratory variability might be a true

reflection of the unpredictable response observed in some children using CPAP (Hoffstein et al., 1992).

The trend of lower fR and increased T_i and T_e in 2-week-old Bmp7^{ncko} mice (Fig. S3), a time prior to structural nasal abnormalities being established, is suggestive that lack of Bmp7 in neural crest during embryonic development may affect developmental processes that only later manifest as phenotypic changes. Hence, the structural abnormalities may be a consequence of the inability to repair and recover and grow during the growth spurt (after 3 weeks in mice). Additionally, the understanding that altered cellular and molecular processes in the human body precede structural abnormalities later in life (Gomes et al., 2012) reaffirms the plasticity of the human body as well as the notion that nasal septum deviation and its consequences establish gradually and not overnight. Thus, better understanding of the underlying genetic alterations associated with nasal airway obstruction will assist in effective management and treatment of the obstruction along with its associated co-morbidities.

The Bmp7^{ncko} model may be used to further investigate the origin of mixed apneas in individuals with craniofacial or neural crest abnormalities. The inability to use craniofacial abnormalities and degree of nasal septum deviation as predictors for the severity of upper airway obstruction and relative contribution of the different apneas is an accurate reflection of the challenges clinicians face in determining/diagnosing using CT scans whether children with nasal obstruction will develop SRBD and require further intervention (Baddam et al., 2020).

Several biomarkers such as kallikrein-1, uromodulin, urocortin-3 and orosomucoid-1 have been proposed as diagnostic markers for pediatric OSA in children although their sensitivity and specificity is yet to be fully understood (De Luca Canto et al., 2015). Using a limited quantitative metabolomics approach, we tested whether this model can be used to identify potential biomarkers for airway obstruction. From screening of 154 metabolites, we observed a significant increase in hydroxyproline. This metabolite has been used as an index of total collagen degradation (Krane et al., 1977) but more recently

has been directly associated with hypoxia in hepatocellular carcinoma (Tang et al., 2018). In that study, hydroxyproline was part of the metabolic axis promoting cell survival through modulating hypoxia inducing factor 1 alpha (HIF1α). Although arterial partial pressure of O_2 (paO_2) was not directly measured in our study, the increase in hydroxyproline may suggest, in addition to reduced physical activity, that the $Bmp7^{ncko}$ mice experience episodes of hypoxia. $Bmp7^{ncko}$ mice showed a decrease with age in the ability to sustain a physical exercise such as running on a treadmill. This may be in indication of their inability to ventilate efficiently. Similarly, a reduced exercise capacity was also observed in children with OSA (Evans et al., 2014). In $Bmp7^{ncko}$ mice, the nasal airway obstruction is likely to be present both during active and rest phases. OSA has been shown to have wider systemic consequences including bone remodeling (Eimar et al., 2016). A reduction in bone mineral density indicative of changes to bone remodelling has been previously identified in children with OSA (Eimar et al., 2019), but it was not clear whether hypoxia affected bone remodelling or vice-versa. Based on our findings, we propose that altered bone metabolism is part of the congenital abnormalities and hypoxia may be a consequence of altered craniofacial growth.

Our observations on $Bmp7^{ncko}$ mice shed new light on the etiology of nasal airway obstruction as a consequence of insufficient midfacial growth. Midfacial hypoplasia on its own cannot predict nor determine the severity of SRBD highlighting the need to carefully investigate craniofacial abnormalities in children. We find that various anomalies in craniofacial structures synergistically predispose to upper airway obstruction. The primary reason for these malformations appears to be altered cartilage and bone development. Although the nasal septum, cranial base and nasal bones grow as a developmental unit, the relative contribution of individual components varies even in this genetically defined model. Environmental factors do play a role, although this has not been well studied yet. For this reason, onset and severity of upper airway obstruction remains largely unpredictable. Although hypoxic ventilatory response appears largely intact, an increased number of post-sigh apneas events and alterations in body temperature during normoxia

and hypoxia suggest the involvement of the central network for respiratory and thermoregulatory control in the features of the Bmp7^{ncko} mice model. At present it is not possible to distinguish whether this is a systemic consequence of upper airway obstruction or due to neural crest-specific roles of Bmp7 outside of bone/cartilage. The multifactorial etiology and presence of mixed apneas reflects the challenges clinicians face in treating complex cases of pediatric OSA, warranting an appropriate genetic model for further study. We have shown that this model can be used for the identification of potential predictive biomarkers to help identify which children with craniofacial malformations are likely to develop SRBD.

In summary, this study demonstrates that Bmp7^{ncko} mouse can be used to identify molecular mechanisms underlying craniofacial abnormalities resulting in nasal airway obstruction to better understand the genetic component contributing to obstruction in children with SRBD.

Methods

Animals

All animal experiments were approved by the Research Ethics Office of the University of Alberta (Animal Use and Care Committee; protocol AUP1149), in compliance with guidelines by the Canadian Council of Animal Care. Mouse lines were kept on a C57Bl/6J background at the animal facility of the University of Alberta. Bmp7$^{fl/fl}$ mice (Zouvelou et al., 2009) (Bmp7^{ctrl}) were crossed to Wnt1-Cre mice, Tg(Wnt1-cre)11Rth, for neural crest–specific deletion of Bmp7(Bmp7$^{fl/fl}$:Wnt1-Cre) (Bmp7^{ncko}). Mice were genotyped using polymerase chain reaction (PCR) with DNA obtained from tissue biopsies (Zouvelou et al., 2009).

Micro-Computed Tomography

For micro-computed tomography (µCT), $Bmp7^{ctrl}$ and $Bmp7^{ncko}$ mice were scanned using MILabs µCT at the School of Dentistry, University of Alberta. The mice were perfused with 4% PFA and mouse heads were subsequently fixed in 4% PFA for another 24 hrs prior to scanning. The following parameters were applied for scanning: voltage = 50kV; current = 0.24mA; and exposure time = 75ms. Scans were reconstructed at a voxel size of 25µm. The µCT- based skull reconstructions were used for anatomical comparison of the heads. Landmarks were placed on the skulls and defined angles/lengths were collected to quantify craniofacial differences (Fig. S1). Reconstructed scans were analyzed using AMIRA (Life Technologies) independently by one rater in triplicate, each time placing landmarks anew and collecting measurements.

Whole Body Plethysmography experimental design

Animals were placed individually in the whole-body plethysmography chamber that was initially flushed with room air (21% O_2) for an acclimation period of 30 to 40 min. $\dot{V}_E$ and $\dot{V}O_2$ were then recorded during baseline (normoxic conditions, 21% O_2 and N_2 balance) for 150 min to guarantee mice would go through the sleep-awake cycle, followed by 20 min exposure to hypoxia (10% O_2 and N_2 balance), allowed to recover to normoxia values for 60 min, followed by 20 min exposure to hyperoxia (40% O_2). Gas mixtures were provided by a gas mixing system (GSM-3 Gas Mixer; CWE Inc., Ardmore, PA, USA). Respiratory and metabolic variables reported represent average values measured during 150 min of normoxia, between 0 to 5 min and 10 to 15 min of hypoxia, the last 10 min of recovery period and between 10 to 15 min of hyperoxia. Body temperature was measured before placing the mice into the chamber, 1 min after hypoxia exposure, at 45 min of recovery period in normoxia, and at the end of hyperoxia.

Measurements of ventilation, O_2 consumption and body temperature

Ventilation was measured using the open flow whole-body plethysmography method (Seifert et al., 2000). The mice were placed in a 100 mL or 200mL volume chamber, depending on the mice's body mass, through which gas flow was maintained at rates of 150 and 300 mL/min, respectively (Lighton, 2008). In this system, the heating and humidification of the air that occurs with rhythmic inspiration and expiration of air causes pressure changes in the chamber that were detected with the differential pressure transducer (Validyne Engineering, Northridge, CA, USA). The pressure signal was acquired using PowerLab System (ADInstruments, Sydney, Australia) and sampled at 200 Hz. Data were analyzed using the data analysis software, LabChart (PowerLab System, ADInstruments/ LabChart Software, version 8, Sydney, Australia). The system was calibrated with injections of 0.25 mL into the plethysmography chamber at the same rate as breathing rate. Tidal volume (V_T) was calculated with the appropriate formula (Drorbaugh and Fenn, 1955): $V_T = V_K \times (P_T/P_K) \times T_C \times (P_B - P_C) / Tb \times (P_B - P_C) - T_A \times (P_B - P_R)$, where P_T is the pressure deflection associated with each V_T, P_K is the pressure deflection associated with the injection of the calibration volume (V_K), T_A is the air temperature in the animal chamber, P_B is the barometric pressure, P_C is the water vapor pressure in the animal chamber, Tb is the body temperature (in Kelvin), and P_R is the water vapor pressure at Tb. Ventilation ($\dot{V}_E$) was calculated as the product of respiratory frequency (fR) and tidal volume (V_T). P_C and P_R were calculated indirectly using appropriate tables (Dejours, 1981). All variables were normalized to body mass. Body temperature was measured using a rectal probe (Physiosuite, Kent Scientific, Torrington, CT, USA). Metabolic rate (O_2 consumption, $\dot{V}O_2$) was measured using pull mode indirect calorimetry (Cummings et al., 2011; Mortola, 1984). An O_2 analyzer pump (ADInstruments, Sydney, Australia) was connected to the outflow of the chamber, where sub sampled air was dried through a small drying column (Drierite, Sigma Aldrich, St. Louis, MO, USA) before passing to the analyzer. The gas was continuously sampled (1000 Hz) by the O_2 and CO_2 analyzers and the fraction of O_2 and CO_2 in the inflow and outflow gas was recorded via PowerLab

(System, ADInstruments / LabChart Software, version 8, Sidney, Australia). O_2 consumption ($\dot{V}O_2$) was calculated based on the following equation (Depocas and Hart, 1957; Lighton, 2008): $\dot{V}O_2 = [FR_e (FiO_2 – FeO_2) – FiO_2 (FeCO_2 – FiCO_2)]/1 – FiO_2$ where FR_e is the excurrent flow rate; FiO_2 is the inflow O_2 fraction; FeO_2 is the outflow O_2 fraction; $FiCO_2$ is the inflow CO_2 fraction; $FeCO_2$ is the outflow CO_2 fraction. $\dot{V}O_2$ was normalized to body mass (in Kg) and the values reported under STPD (standard conditions of temperature, pressure and dry air).

Spontaneous Apnea, Sigh and Post-sigh Apnea analysis

Spontaneous apneas were defined as at least 2 missing breath cycles which corresponds to pauses of 1 second or longer in the breathing recordings depending on the breathing frequency of each mouse. Sighs were defined as an increased breath at least twice a normal breath volume. Post-sigh apneas were defined as apneas that occurred within 20 seconds from the occurrence of a sigh (Yamauchi et al., 2008). Post-sigh apneas were further differentiated as 1) sighs followed by < 2 apneas, i.e., sigh not followed by apnea, or accompanied by one apnea; and 2) sighs followed by ≥ 2 apneas, separated at least by one breath.

Comprehensive Lab Monitoring System (CLAMS)

CLAMS (Oxymax/CLAMS; Columbus Instruments, Columbus, OH) was used to measure delta oxygen and respiratory exchange ratio (RER= $\dot{V}CO_2$ / $\dot{V}O_2$) in vivo. A previously described protocol was used to conduct these experiments (Koonen et al., 2010). 1-month old mice (n=5/genotype) were monitored for 24 hrs to measure under both light (inactive) and dark (active) cycles for 12 hours each.

Metabolomics – combined direct flow injection and liquid chromatography with tandem mass spectrometry (LC-MS/MS) compound identification and quantification

A targeted quantitative metabolomics approach was used to analyze the blood serum samples of $Bmp7^{ctrl}$ and $Bmp7^{ncko}$ mice (n=5 mice/genotype) using a combination of direct injection mass spectrometry (AbsoluteIDQ™ Kit) with a reverse-phase liquid chromatography with tandem mass spectrometry (LC-MS/MS) Kit (BIOCRATES LifeSciences AG, Austria). This kit, in combination with an ABI 4000 Q-Trap (Applied Biosystems/MDS Sciex) mass spectrometer combines the derivatization and extraction of analytes, and the selective mass-spectrometric detection using multiple reaction monitoring (MRM) pairs. Isotope-labeled internal standards and other internal standards are integrated in Kit plate filter for metabolite quantification. All the serum samples were analyzed with the AbsoluteIDQ kit using the protocol described in the AbsoluteIDQ user manual. Briefly, serum samples were thawed on ice and were vortexed and centrifuged at 13,000x g. 10 µL of each serum sample was loaded onto the center of the filter on the upper 96-well kit plate and dried in a stream of nitrogen. Subsequently, 20 µL of a 5% solution of phenyl-isothiocyanate was added for derivatization. After incubation, the filter spots were dried again using an evaporator. Extraction of the metabolites was then achieved by adding 300 µL methanol containing 5mM ammonium acetate. The extracts were obtained by centrifugation into the lower 96-deep well plate, followed by a dilution step with kit MS running solvent. Mass spectrometric analysis was performed on an API4000 Qtrap® tandem mass spectrometry instrument (Applied Biosystems/MDS Analytical Technologies, Foster City, CA) equipped with a solvent delivery system. The samples were delivered to the mass spectrometer by a LC method followed by a direct injection (DI) method. The Biocrates MetIQ software was used to control the entire assay workflow, from sample registration to automated calculation of metabolite concentrations to the export of data into other data analysis programs. A targeted profiling scheme was used to quantitatively screen for known small molecule metabolites using multiple reaction monitoring, neutral

loss and precursor ion scans. Significantly altered metabolites between $Bmp7^{ctrl}$ and $Bmp7^{ncko}$ mice were identified via a two-tailed t-test.

Treadmill Endurance Test

Mice were run on the Exer 3/6 treadmill with a variable speed controller (Columbus Instruments) (Dougherty *et al.*, 2016). For endurance, after initial training, mice were familiarized with a speed of 3 meters (m)/minute for 2 minutes(min), increasing every 2 minutes by 1 m/min. Distance recording starts at a speed of 6 m/min for 6 minutes, followed by 8 m/min for 10 minutes, subsequent of which the speed is increased by 2 m/min every 3 minutes. Time is recorded when animals tire and the distance run is calculated. For speed testing, mice were familiarized at 7 m/min for 5 minutes, and then speed was set to 12m/min for up to 5 minutes. Mice were video recorded. For endurance testing, 4 mice/genotype were recorded. For speed testing, 5 mice/genotype were recorded.

Statistics

Results are expressed as means ± SD. For the morphometric µCT, CLAMS and metabolomics analyses, significant differences between $Bmp7^{ctrl}$ and $Bmp7^{ncko}$ mice were estimated by a two-tailed independent t-test and differences were considered statistically significant when $p < 0.05$. Morphometric µCT measurements were conducted by one rater in triplicate. Intra-rater reliability was assessed wherever possible by intraclass correlation (ICC) calculation based on 6 mice at 1-month time point with ICC values greater than 0.9 being considered as excellent reliability (Table S4). For findings from whole body plethysmograph, a statistical comparison of means was performed to compare respiratory (V_T, fR, $\dot{V}_E$, number of SA and sighs, % PSA), metabolic ($\dot{V}O_2$, $\dot{V}_E/\dot{V}O_2$) and body temperature (Tb) variables between the experimental groups ($Bmp7^{ctrl}$, $Bmp7^{ncko\,(r)}$ and $Bmp7^{ncko\,(a)}$ mice) and gas exposure (21% O_2, 10% O_2 and 40% O_2). Two-way repeated measures ANOVA and Holm-Sidak post-test were used for each of these comparisons. The

normoxic breath cycle duration (T_{TOT}), inspiratory (T_i) and expiratory (T_e) times comparison between the experimental groups ($Bmp7^{ctrl}$, $Bmp7^{ncko\,(r)}$ and $Bmp7^{ncko\,(a)}$ mice) were analyzed using One-way ANOVA. Values of $p < 0.05$ were considered significant. Values were expressed as mean±SD.

Acknowledgements

The authors would like to acknowledge the microCT facility of the School of Dentistry, University of Alberta.

Competing Interests

The authors declare no competing interests.

Funding

This work has been supported by the Women and Children Health Research Institute (WCHRI) Innovation Grant (DG), the American Association of Orthodontists Foundation (CFM and DG) and WCHRI Postdoctoral Fellowship Program (VB).

Data Availability

The datasets used and/or analyzed during the current study are available from the corresponding author on reasonable request.

Author contributions

PB: conceptualization, data acquisition, data analysis, drafting of manuscript, critical revision of the manuscript and approval of the article

DMR: data acquisition, data analysis, drafting of manuscript, critical revision of the manuscript and approval of the article

VB: data acquisition, data analysis, drafting of manuscript, critical revision of the manuscript and approval of the article

FE: data acquisition and approval of the article

CTB: critical revision of the manuscript and approval of the article

RM: data acquisition, critical revision of the manuscript and approval of the article

DSW: data acquisition, critical revision of the manuscript and approval of the article

AB: data acquisition and approval of the article

JM: data analysis, critical revision of the manuscript and approval of the article

CFM: funding acquisition, data analysis, critical revision of the manuscript and approval of the article

SP: concept/design, data analysis, critical revision of the manuscript and approval of the article

DG: concept/design, funding acquisition, data acquisition, data analysis, drafting of manuscript, critical revision of the manuscript and approval of the article

References

Agrawal, A., Singh, S.K., Singh, V.P., Murphy, E., Parikh, I., 2008. Partitioning of nasal and pulmonary resistance changes during noninvasive plethysmography in mice. J. Appl. Physiol. 105, 1975–1979. https://doi.org/10.1152/japplphysiol.90700.2008

Almendros, I., Farré, R., Planas, A.M., Torres, M., Bonsignore, M.R., Navajas, D., Montserrat, J.M., 2011. Tissue oxygenation in brain, muscle, and fat in a rat model of sleep apnea: differential effect of obstructive apneas and intermittent hypoxia. Sleep 34, 1127–1133. https://doi.org/10.5665/SLEEP.1176

Annese, V., Navarro-Guerrero, E., Rodríguez-Prieto, I., Pardal, R., 2017. Physiological Plasticity of Neural-Crest-Derived Stem Cells in the Adult Mammalian Carotid Body. Cell Rep 19, 471–478. https://doi.org/10.1016/j.celrep.2017.03.065

Baddam, P., Bussolaro, C.-T., Flores-Mir, C., Graf, D., 2020. Nasal cavity structural anomalies among children at high risk of sleep-disordered breathing: an exploratory cone-beam computed tomography study. American Journal of Orthodontics & Dentofacial Orthopedics In Press.

Bastianini, S., Alvente, S., Berteotti, C., Bosi, M., Lo Martire, V., Silvani, A., Valli, A., Zoccoli, G., 2019. Post-sigh sleep apneas in mice: Systematic review and data-driven definition. J Sleep Res 28, e12845. https://doi.org/10.1111/jsr.12845

Berger, S., Pho, H., Fleury-Curado, T., Bevans-Fonti, S., Younas, H., Shin, M.-K., Jun, J.C., Anokye-Danso, F., Ahima, R.S., Enquist, L.W., Mendelowitz, D., Schwartz, A.R., Polotsky, V.Y., 2019. Intranasal Leptin Relieves Sleep-disordered Breathing in Mice with Diet-induced Obesity. Am. J. Respir. Crit. Care Med. 199, 773–783. https://doi.org/10.1164/rccm.201805-0879OC

Bozzini, M.F.R., Di Francesco, R.C., 2016. Managing obstructive sleep apnoea in children: the role of craniofacial morphology. Clinics (Sao Paulo) 71, 664–666. https://doi.org/10.6061/clinics/2016(11)08

Brennick, M.J., Pack, A.I., Ko, K., Kim, E., Pickup, S., Maislin, G., Schwab, R.J., 2009. Altered upper airway and soft tissue structures in the New Zealand Obese mouse. Am. J.

Respir. Crit. Care Med. 179, 158–169. https://doi.org/10.1164/rccm.200809-1435OC

Carithers, J.S., Gebhart, D.E., Williams, J.A., 1987. Postoperative risks of pediatric tonsilloadenoidectomy. Laryngoscope 97, 422–429. https://doi.org/10.1288/00005537-198704000-00004

Chemelli, R.M., Willie, J.T., Sinton, C.M., Elmquist, J.K., Scammell, T., Lee, C., Richardson, J.A., Williams, S.C., Xiong, Y., Kisanuki, Y., Fitch, T.E., Nakazato, M., Hammer, R.E., Saper, C.B., Yanagisawa, M., 1999. Narcolepsy in orexin Knockout Mice: Molecular Genetics of Sleep Regulation. Cell 98, 437–451. https://doi.org/10.1016/S0092-8674(00)81973-X

Choe, Y., Kozlova, A., Graf, D., Pleasure, S.J., 2013. Bone morphogenic protein signaling is a major determinant of dentate development. J. Neurosci. 33, 6766–6775. https://doi.org/10.1523/JNEUROSCI.0128-13.2013

Chopra, S., Polotsky, V.Y., Jun, J.C., 2016. Sleep Apnea Research in Animals. Past, Present, and Future. Am J Respir Cell Mol Biol 54, 299–305. https://doi.org/10.1165/rcmb.2015-0218TR

Cielo, C.M., Montalva, F.M., Taylor, J.A., 2016. Craniofacial disorders associated with airway obstruction in the neonate. Semin Fetal Neonatal Med 21, 254–262. https://doi.org/10.1016/j.siny.2016.03.001

Clark, D.W., Del Signore, A.G., Raithatha, R., Senior, B.A., 2018. Nasal airway obstruction: Prevalence and anatomic contributors. Ear Nose Throat J 97, 173–176. https://doi.org/10.1177/014556131809700615

Cummings, K.J., Hewitt, J.C., Li, A., Daubenspeck, J.A., Nattie, E.E., 2011. Postnatal loss of brainstem serotonin neurones compromises the ability of neonatal rats to survive episodic severe hypoxia. J. Physiol. (Lond.) 589, 5247–5256. https://doi.org/10.1113/jphysiol.2011.214445

Davis, E.M., O'Donnell, C.P., 2013. RODENT MODELS OF SLEEP APNEA. Respir Physiol Neurobiol 188, 355–361. https://doi.org/10.1016/j.resp.2013.05.022

De Luca Canto, G., Pachêco-Pereira, C., Aydinoz, S., Major, P.W., Flores-Mir, C., Gozal, D., 2015. Biomarkers associated with obstructive sleep apnea: A scoping review. Sleep Med Rev 23, 28–45. https://doi.org/10.1016/j.smrv.2014.11.004

Dejours, P., 1981. Principles of Comparative Respiratory Physiology. Elsevier/North-Holland Biomedical Press.

Depocas, F., Hart, J.S., 1957. Use of the Pauling oxygen analyzer for measurement of oxygen consumption of animals in open-circuit systems and in a short-lag, closed-circuit apparatus. J Appl Physiol 10, 388–392. https://doi.org/10.1152/jappl.1957.10.3.388

Dewan, N.A., Nieto, F.J., Somers, V.K., 2015. Intermittent Hypoxemia and OSA. Chest 147, 266–274. https://doi.org/10.1378/chest.14-0500

Diniz Behn, C.G., Klerman, E.B., Mochizuki, T., Lin, S.-C., Scammell, T.E., 2010. Abnormal Sleep/Wake Dynamics in Orexin Knockout Mice. Sleep 33, 297–306.

Drorbaugh, J.E., Fenn, W.O., 1955. A barometric method for measuring ventilation in newborn infants. Pediatrics 16, 81–87.

Eimar, H., Al-Saleh, M. a. Q., Cortes, A.R.G., Gozal, D., Graf, D., Flores-Mir, C., 2019. Sleep-Disordered Breathing Is Associated with Reduced Mandibular Cortical Width in Children. JDR Clin Trans Res 4, 58–67. https://doi.org/10.1177/2380084418776906

Eimar, H., Tamimi, F., Retrouvey, J.-M., Rauch, F., Aubin, J.E., McKee, M.D., 2016. Craniofacial and Dental Defects in the Col1a1Jrt/+ Mouse Model of Osteogenesis Imperfecta. J. Dent. Res. 95, 761–768. https://doi.org/10.1177/0022034516637045

Evans, C.A., Selvadurai, H., Baur, L.A., Waters, K.A., 2014. Effects of Obstructive Sleep Apnea and Obesity on Exercise Function in Children. Sleep 37, 1103–1110. https://doi.org/10.5665/sleep.3770

Farré, R., Montserrat, J.M., Gozal, D., Almendros, I., Navajas, D., 2018. Intermittent Hypoxia Severity in Animal Models of Sleep Apnea. Front Physiol 9. https://doi.org/10.3389/fphys.2018.01556

Farré, R., Rotger, M., Montserrat, J.M., Calero, G., Navajas, D., 2003. Collapsible upper airway segment to study the obstructive sleep apnea/hypopnea syndrome in rats. Respir Physiol Neurobiol 136, 199–209. https://doi.org/10.1016/s1569-9048(03)00082-x

Finkelstein, Y., Wexler, D., Berger, G., Nachmany, A., Shapiro-Feinberg, M., Ophir, D., 2000. Anatomical Basis of Sleep-Related Breathing Abnormalities in Children With Nasal Obstruction. Arch Otolaryngol Head Neck Surg 126, 593–600. https://doi.org/10.1001/archotol.126.5.593

Fletcher, E.C., Lesske, J., Behm, R., Miller, C.C., Stauss, H., Unger, T., 1992. Carotid chemoreceptors, systemic blood pressure, and chronic episodic hypoxia mimicking sleep apnea. J. Appl. Physiol. 72, 1978–1984. https://doi.org/10.1152/jappl.1992.72.5.1978

Gabryelska, A., Łukasik, Z.M., Makowska, J.S., Białasiewicz, P., 2018. Obstructive Sleep Apnea: From Intermittent Hypoxia to Cardiovascular Complications via Blood Platelets. Front Neurol 9, 635. https://doi.org/10.3389/fneur.2018.00635

Gangopadhyay, N., Mendonca, D.A., Woo, A.S., 2012. Pierre Robin Sequence. Semin Plast Surg 26, 76–82. https://doi.org/10.1055/s-0032-1320065

Gipson, K., Lu, M., Kinane, T.B., 2019. Sleep-Disordered Breathing in Children. Pediatr Rev 40, 3–13. https://doi.org/10.1542/pir.2018-0142

Gleadhill, I.C., Schwartz, A.R., Schubert, N., Wise, R.A., Permutt, S., Smith, P.L., 1991. Upper airway collapsibility in snorers and in patients with obstructive hypopnea and apnea. Am. Rev. Respir. Dis. 143, 1300–1303. https://doi.org/10.1164/ajrccm/143.6.1300

Gomes, J., Finlay, M., Ahmed, A.K., Ciaccio, E.J., Asimaki, A., Saffitz, J.E., Quarta, G., Nobles, M., Syrris, P., Chaubey, S., McKenna, W.J., Tinker, A., Lambiase, P.D., 2012. Electrophysiological abnormalities precede overt structural changes in arrhythmogenic right ventricular cardiomyopathy due to mutations in

desmoplakin-A combined murine and human study. Eur Heart J 33, 1942–1953. https://doi.org/10.1093/eurheartj/ehr472

Gozal, D., 1998. Sleep-disordered breathing and school performance in children. Pediatrics 102, 616–620. https://doi.org/10.1542/peds.102.3.616

Gozal, D., Daniel, J.M., Dohanich, G.P., 2001. Behavioral and anatomical correlates of chronic episodic hypoxia during sleep in the rat. J. Neurosci. 21, 2442–2450.

Harkema, J.R., Morgan, K.T., 1996. Normal Morphology of the Nasal Passages in Laboratory Rodents, in: Jones, T.C., Dungworth, D.L., Mohr, U. (Eds.), Respiratory System, Monographs on Pathology of Laboratory Animals. Springer, Berlin, Heidelberg, pp. 3–17. https://doi.org/10.1007/978-3-642-61042-4_1

Hendricks, J.C., Kline, L.R., Kovalski, R.J., O'Brien, J.A., Morrison, A.R., Pack, A.I., 1987. The English bulldog: a natural model of sleep-disordered breathing. J. Appl. Physiol. 63, 1344–1350. https://doi.org/10.1152/jappl.1987.63.4.1344

Hoeve, H.L., Joosten, K.F., van den Berg, S., 1999. Management of obstructive sleep apnea syndrome in children with craniofacial malformation. Int. J. Pediatr. Otorhinolaryngol. 49 Suppl 1, S59-61. https://doi.org/10.1016/s0165-5876(99)00134-2

Hoffstein, V., Viner, S., Mateika, S., Conway, J., 1992. Treatment of obstructive sleep apnea with nasal continuous positive airway pressure. Patient compliance, perception of benefits, and side effects [WWW Document]. The American review of respiratory disease. https://doi.org/10.1164/ajrccm/145.4_Pt_1.841

Hong, M., Krauss, R.S., 2012. Cdon mutation and fetal ethanol exposure synergize to produce midline signaling defects and holoprosencephaly spectrum disorders in mice. PLoS Genet. 8, e1002999. https://doi.org/10.1371/journal.pgen.1002999

Hsu, D.W., Suh, J.D., 2018. Anatomy and Physiology of Nasal Obstruction. Otolaryngologic Clinics of North America, Nasal Airway Obstruction 51, 853–865. https://doi.org/10.1016/j.otc.2018.05.001

Huang, W., Olsen, B.R., 2015. Skeletal defects in Osterix-Cre transgenic mice. Transgenic Res. 24, 167–172. https://doi.org/10.1007/s11248-014-9828-6

Iida, M., Murakami, T., Ishida, K., Mizuno, A., Kuwajima, M., Shima, K., 1996. Substitution at codon 269 (glutamine --> proline) of the leptin receptor (OB-R) cDNA is the only mutation found in the Zucker fatty (fa/fa) rat. Biochem. Biophys. Res. Commun. 224, 597–604. https://doi.org/10.1006/bbrc.1996.1070

Ishizuka, T., Ernsberger, P., Liu, S., Bedol, D., Lehman, T.M., Koletsky, R.J., Friedman, J.E., 1998. Phenotypic consequences of a nonsense mutation in the leptin receptor gene (fak) in obese spontaneously hypertensive Koletsky rats (SHROB). J. Nutr. 128, 2299–2306. https://doi.org/10.1093/jn/128.12.2299

Khurana, A., Thach, B.T., 1996. Effects of upper airway stimulation on swallowing, gasping, and autoresuscitation in hypoxic mice. Journal of Applied Physiology 80, 472–477. https://doi.org/10.1152/jappl.1996.80.2.472

Koonen, D.P.Y., Sung, M.M.Y., Kao, C.K.C., Dolinsky, V.W., Koves, T.R., Ilkayeva, O., Jacobs, R.L., Vance, D.E., Light, P.E., Muoio, D.M., Febbraio, M., Dyck, J.R.B., 2010. Alterations in skeletal muscle fatty acid handling predisposes middle-aged mice to diet-induced insulin resistance. Diabetes 59, 1366–1375. https://doi.org/10.2337/db09-1142

Kouskoura, T., El Fersioui, Y., Angelini, M., Graf, D., Katsaros, C., Chiquet, M., 2016. Dislocated Tongue Muscle Attachment and Cleft Palate Formation. J. Dent. Res. 95, 453–459. https://doi.org/10.1177/0022034515621869

Kouskoura, T., Kozlova, A., Alexiou, M., Blumer, S., Zouvelou, V., Katsaros, C., Chiquet, M., Mitsiadis, T.A., Graf, D., 2013. The etiology of cleft palate formation in BMP7-deficient mice. PLoS ONE 8, e59463. https://doi.org/10.1371/journal.pone.0059463

Krane, S.M., Kantrowitz, F.G., Byrne, M., Pinnell, S.R., Singer, F.R., 1977. Urinary excretion of hydroxylysine and its glycosides as an index of collagen degradation. J. Clin. Invest. 59, 819–827. https://doi.org/10.1172/JCI108704

Lee, R.W.W., Vasudavan, S., Hui, D.S., Prvan, T., Petocz, P., Darendeliler, M.A., Cistulli, P.A., 2010. Differences in Craniofacial Structures and Obesity in Caucasian and Chinese Patients with Obstructive Sleep Apnea. Sleep 33, 1075–1080.

Leger, D., Bayon, V., Laaban, J.P., Philip, P., 2012. Impact of sleep apnea on economics. Sleep Med Rev 16, 455–462. https://doi.org/10.1016/j.smrv.2011.10.001

Lewis, A.E., Vasudevan, H.N., O'Neill, A.K., Soriano, P., Bush, J.O., 2013. The widely used Wnt1-Cre transgene causes developmental phenotypes by ectopic activation of Wnt signaling. Dev Biol 379, 229–234. https://doi.org/10.1016/j.ydbio.2013.04.026

Li, P., Janczewski, W.A., Yackle, K., Kam, K., Pagliardini, S., Krasnow, M.A., Feldman, J.L., 2016. The peptidergic control circuit for sighing. Nature 530, 293–297. https://doi.org/10.1038/nature16964

Lighton, J.R.B., 2008. Measuring Metabolic Rates: A Manual for Scientists. Oxford University Press.

Marulanda, J., Eimar, H., McKee, M.D., Berkvens, M., Nelea, V., Roman, H., Borrás, T., Tamimi, F., Ferron, M., Murshed, M., 2017. Matrix Gla protein deficiency impairs nasal septum growth, causing midface hypoplasia. J. Biol. Chem. 292, 11400–11412. https://doi.org/10.1074/jbc.M116.769802

Mehta, V., Vasu, T.S., Phillips, B., Chung, F., 2013. Obstructive sleep apnea and oxygen therapy: a systematic review of the literature and meta-analysis. J Clin Sleep Med 9, 271–279. https://doi.org/10.5664/jcsm.2500

Milanesi, J. de M., Berwig, L.C., Schuch, L.H., Ritzel, R.A., Silva, A.M.T. da, Corrêa, E.C.R., 2019. Nasal patency and otorhinolaryngologic-orofacial features in children. Braz J Otorhinolaryngol 85, 83–91. https://doi.org/10.1016/j.bjorl.2017.10.014

Morgenthaler, T.I., Kapen, S., Lee-Chiong, T., Alessi, C., Boehlecke, B., Brown, T., Coleman, J., Friedman, L., Kapur, V., Owens, J., Pancer, J., Swick, T., Standards of Practice Committee, American Academy of Sleep Medicine, 2006. Practice parameters for the medical therapy of obstructive sleep apnea. Sleep 29, 1031–1035.

Mortola, J.P., 1984. Breathing pattern in newborns. J Appl Physiol Respir Environ Exerc Physiol 56, 1533–1540. https://doi.org/10.1152/jappl.1984.56.6.1533

Moss, I.R., 2000. Respiratory responses to single and episodic hypoxia during development: mechanisms of adaptation. Respir Physiol 121, 185–197. https://doi.org/10.1016/s0034-5687(00)00127-4

Niaki, S.E.A., Shafaroodi, H., Ghasemi, M., Shakiba, B., Fakhimi, A., Dehpour, A.R., 2008. Mouth breathing increases the pentylenetetrazole-induced seizure threshold in mice: a role for ATP-sensitive potassium channels. Epilepsy Behav 13, 284–289. https://doi.org/10.1016/j.yebeh.2008.04.013

O'Donnell, C.P., Tankersley, C.G., Polotsky, V.P., Schwartz, A.R., Smith, P.L., 2000. Leptin, obesity, and respiratory function. Respir Physiol 119, 163–170. https://doi.org/10.1016/s0034-5687(99)00111-5

Pacheco, M.C.T., Fiorott, B.S., Finck, N.S., de Araújo, M.T.M., 2015. Craniofacial changes and symptoms of sleep-disordered breathing in healthy children. Dental Press J Orthod 20, 80–87. https://doi.org/10.1590/2176-9451.20.3.080-087.oar

Pavan, W.J., Raible, D.W., 2012. Specification of neural crest into sensory neuron and melanocyte lineages. Dev Biol 366, 55–63. https://doi.org/10.1016/j.ydbio.2012.02.038

Peña, F., Ramirez, J.-M., 2005. Hypoxia-induced changes in neuronal network properties. Mol. Neurobiol. 32, 251–283. https://doi.org/10.1385/MN:32:3:251

Perlyn, C.A., DeLeon, V.B., Babbs, C., Govier, D., Burell, L., Darvann, T., Kreiborg, S., Morriss-Kay, G., 2006. The craniofacial phenotype of the Crouzon mouse: analysis of a model for syndromic craniosynostosis using three-dimensional MicroCT. Cleft Palate Craniofac. J. 43, 740–748. https://doi.org/10.1597/05-212

Polotsky, M., Elsayed-Ahmed, A.S., Pichard, L., Harris, C.C., Smith, P.L., Schneider, H., Kirkness, J.P., Polotsky, V., Schwartz, A.R., 2012. Effects of leptin and obesity on the upper airway function. J. Appl. Physiol. 112, 1637–1643. https://doi.org/10.1152/japplphysiol.01222.2011

Rosenberg, P., Arlis, H.R., Haworth, R.D., Heier, L., Hoffman, L., LaTrenta, G., 1997. The role of the cranial base in facial growth: experimental craniofacial synostosis in the rabbit. Plast Reconstr Surg 99, 1396–1407. https://doi.org/10.1097/00006534-199704001-00030

Saito, Y., Ezure, K., Kobayashi, M., Ito, M., Saito, K., Osawa, M., 2002. A review of functional and structural components of the respiratory center involved in the arousal response. Sleep Med. 3 Suppl 2, S71-74. https://doi.org/10.1016/s1389-9457(02)00170-3

Sanders, M.H., Moore, S.E., 1983. Inspiratory and expiratory partitioning of airway resistance during sleep in patients with sleep apnea. Am. Rev. Respir. Dis. 127, 554–558. https://doi.org/10.1164/arrd.1983.127.5.554

Schoorlemmer, G.H.M., Rossi, M.V., Tufik, S., Cravo, S.L., 2011. A new method to produce obstructive sleep apnoea in conscious unrestrained rats. Exp. Physiol. 96, 1010–1018. https://doi.org/10.1113/expphysiol.2011.059014

Segklia, A., Seuntjens, E., Elkouris, M., Tsalavos, S., Stappers, E., Mitsiadis, T.A., Huylebroeck, D., Remboutsika, E., Graf, D., 2012. Bmp7 regulates the survival, proliferation, and neurogenic properties of neural progenitor cells during corticogenesis in the mouse. PLoS ONE 7, e34088. https://doi.org/10.1371/journal.pone.0034088

Seifert, E.L., Knowles, J., Mortola, J.P., 2000. Continuous circadian measurements of ventilation in behaving adult rats. Respir Physiol 120, 179–183. https://doi.org/10.1016/s0034-5687(00)00108-0

Skotko, B.G., Macklin, E.A., Muselli, M., Voelz, L., McDonough, M.E., Davidson, E., Allareddy, V., Jayaratne, Y.S.N., Bruun, R., Ching, N., Weintraub, G., Gozal, D., Rosen, D., 2017. A predictive model for obstructive sleep apnea and Down syndrome. Am. J. Med. Genet. A 173, 889–896. https://doi.org/10.1002/ajmg.a.38137

Strohl, K.P., Thomas, A.J., 2001. Ventilatory behavior and metabolism in two strains of obese rats. Respir Physiol 124, 85–93. https://doi.org/10.1016/s0034-5687(00)00190-0

Suzuki, A., Sangani, D.R., Ansari, A., Iwata, J., 2016. Molecular Mechanisms of Midfacial Developmental Defects. Dev Dyn 245, 276–293. https://doi.org/10.1002/dvdy.24368

Takaya, K., Ogawa, Y., Hiraoka, J., Hosoda, K., Yamori, Y., Nakao, K., Koletsky, R.J., 1996. Nonsense mutation of leptin receptor in the obese spontaneously hypertensive Koletsky rat. Nat. Genet. 14, 130–131. https://doi.org/10.1038/ng1096-130

Tan, A., Cheung, Y.Y., Yin, J., Lim, W.-Y., Tan, L.W.L., Lee, C.-H., 2016. Prevalence of sleep-disordered breathing in a multiethnic Asian population in Singapore: A community-based study. Respirology 21, 943–950. https://doi.org/10.1111/resp.12747

Tang, L., Zeng, J., Geng, P., Fang, C., Wang, Y., Sun, M., Wang, C., Wang, J., Yin, P., Hu, C., Guo, L., Yu, J., Gao, P., Li, E., Zhuang, Z., Xu, G., Liu, Y., 2018. Global Metabolic Profiling Identifies a Pivotal Role of Proline and Hydroxyproline Metabolism in Supporting Hypoxic Response in Hepatocellular Carcinoma. Clin Cancer Res 24, 474–485. https://doi.org/10.1158/1078-0432.CCR-17-1707

Tarasiuk, A., Scharf, S.M., Miller, M.J., 1991. Effect of chronic resistive loading on inspiratory muscles in rats. J. Appl. Physiol. 70, 216–222. https://doi.org/10.1152/jappl.1991.70.1.216

Tarasiuk, A., Segev, Y., 2018. Abnormal Growth and Feeding Behavior in Upper Airway Obstruction in Rats. Front Endocrinol (Lausanne) 9, 298. https://doi.org/10.3389/fendo.2018.00298

Teppema, L.J., Dahan, A., 2010. The ventilatory response to hypoxia in mammals: mechanisms, measurement, and analysis. Physiol. Rev. 90, 675–754. https://doi.org/10.1152/physrev.00012.2009

Trosman, I., Trosman, S.J., 2017. Cognitive and Behavioral Consequences of Sleep Disordered Breathing in Children. Med Sci (Basel) 5. https://doi.org/10.3390/medsci5040030

Veasey, S., 2009. Insight from animal models into the cognitive consequences of adult sleep-disordered breathing. ILAR J 50, 307–311. https://doi.org/10.1093/ilar.50.3.307

Vora, S.R., Camci, E.D., Cox, T.C., 2015. Postnatal Ontogeny of the Cranial Base and Craniofacial Skeleton in Male C57BL/6J Mice: A Reference Standard for Quantitative Analysis. Front Physiol 6, 417. https://doi.org/10.3389/fphys.2015.00417

Wang, Y., Spatz, M.K., Kannan, K., Hayk, H., Avivi, A., Gorivodsky, M., Pines, M., Yayon, A., Lonai, P., Givol, D., 1999. A mouse model for achondroplasia produced by targeting fibroblast growth factor receptor 3. PNAS 96, 4455–4460. https://doi.org/10.1073/pnas.96.8.4455

Wei, X., Thomas, N., Hatch, N.E., Hu, M., Liu, F., 2017. Postnatal Craniofacial Skeletal Development of Female C57BL/6NCrl Mice. Front. Physiol. 8. https://doi.org/10.3389/fphys.2017.00697

Wellman, A., Malhotra, A., Jordan, A.S., Stevenson, K.E., Gautam, S., White, D.P., 2008. Effect of oxygen in obstructive sleep apnea: role of loop gain. Respir Physiol Neurobiol 162, 144–151. https://doi.org/10.1016/j.resp.2008.05.019

Xie, A., Teodorescu, M., Pegelow, D.F., Teodorescu, M.C., Gong, Y., Fedie, J.E., Dempsey, J.A., 2013. Effects of stabilizing or increasing respiratory motor outputs on obstructive sleep apnea. J. Appl. Physiol. 115, 22–33. https://doi.org/10.1152/japplphysiol.00064.2013

Yamauchi, M., Ocak, H., Dostal, J., Jacono, F.J., Loparo, K.A., Strohl, K.P., 2008. Post-sigh breathing behavior and spontaneous pauses in the C57BL/6J (B6) mouse. Respir Physiol Neurobiol 162, 117–125. https://doi.org/10.1016/j.resp.2008.05.003

Yamauchi, M., Tamaki, S., Yoshikawa, M., Ohnishi, Y., Nakano, H., Jacono, F.J., Loparo, K.A., Strohl, K.P., Kimura, H., 2011. Differences in Breathing Patterning During Wakefulness in Patients With Mixed Apnea-Dominant vs Obstructive-Dominant Sleep Apnea. Chest 140, 54–61. https://doi.org/10.1378/chest.10-1082

Zouvelou, V., Luder, H.-U., Mitsiadis, T.A., Graf, D., 2009. Deletion of BMP7 affects the development of bones, teeth, and other ectodermal appendages of the orofacial complex. J. Exp. Zool. B Mol. Dev. Evol. 312B, 361–374. https://doi.org/10.1002/jez.b.21262

Figures

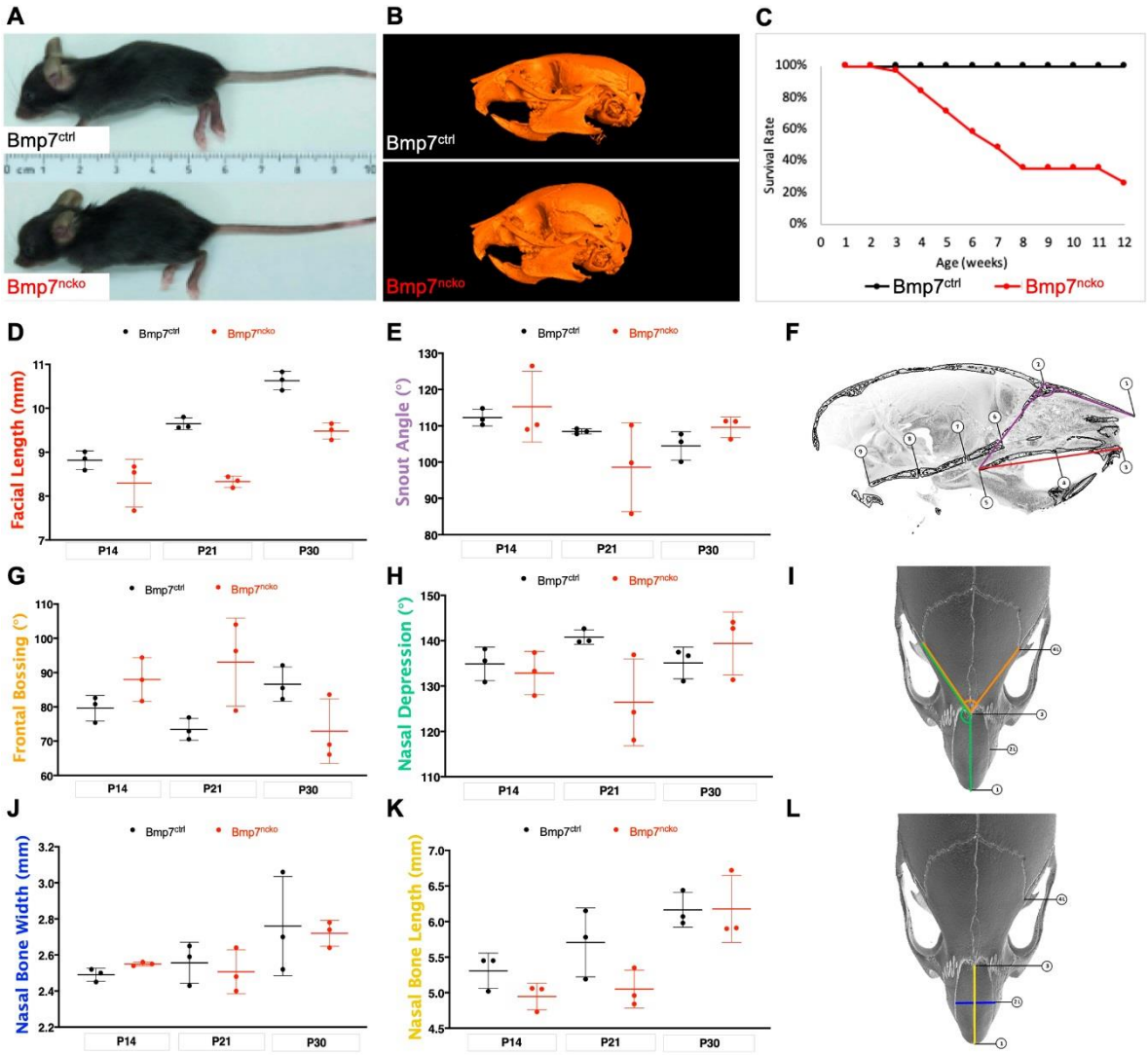

Figure 1. Bmp7^{ncko} mice present with midfacial hypoplasia at 2 weeks which persists with age. (A) Overview of Bmp7 control (Bmp7^{ctrl}) and Bmp7 mutant (Bmp7^{ncko}) mice. **(B)** Micro-computed tomography (µCT) reconstruction of 1-month old mouse skulls. Bmp7^{ncko} skull has a distinctive dished midface when compared with Bmp7^{ctrl}. **(C)** Survival rate plotted against mice age indicating marked decrease in survival of Bmp7^{ncko} mice beginning at 3 weeks with only 30% of Bmp7^{ncko} mice surviving past 8 weeks (n=30). **(D)** Cross-sectional longitudinal morphometric measurement of facial length of Bmp7^{ctrl} (black) and Bmp7^{ncko} (red) skull dimensions at 2 weeks of age (P14), 3 weeks (P21), and 1

month (P30) indicating a shorter facial length in the mutant mice. Landmarks used for this measurement depicted in panel **(F)** in red. **(E)** Snout angle, depicted in panel (F) in purple. **(F)** Midsagittal representation of landmarks used for measurements taken in (D) and (E). **(G)** Frontal bossing angle depicted in panel (I) in orange. **(H)** Average of left and right nasal depression angles, depicted unilaterally in panel (I) in green. **(I**) Superior view diagram of measurements taken in (G) and (H). **(J)** Nasal bone width depicted in panel (L) in blue. **(K)** Nasal bone length depicted in panel (L) in yellow. **(L)** Diagram of measurements taken in (J) and (K). Superior view of skull. For all measurements, n=3/genotype/age. * indicates $p<0.05$. Anatomical description of the landmarks in Fig. S1.

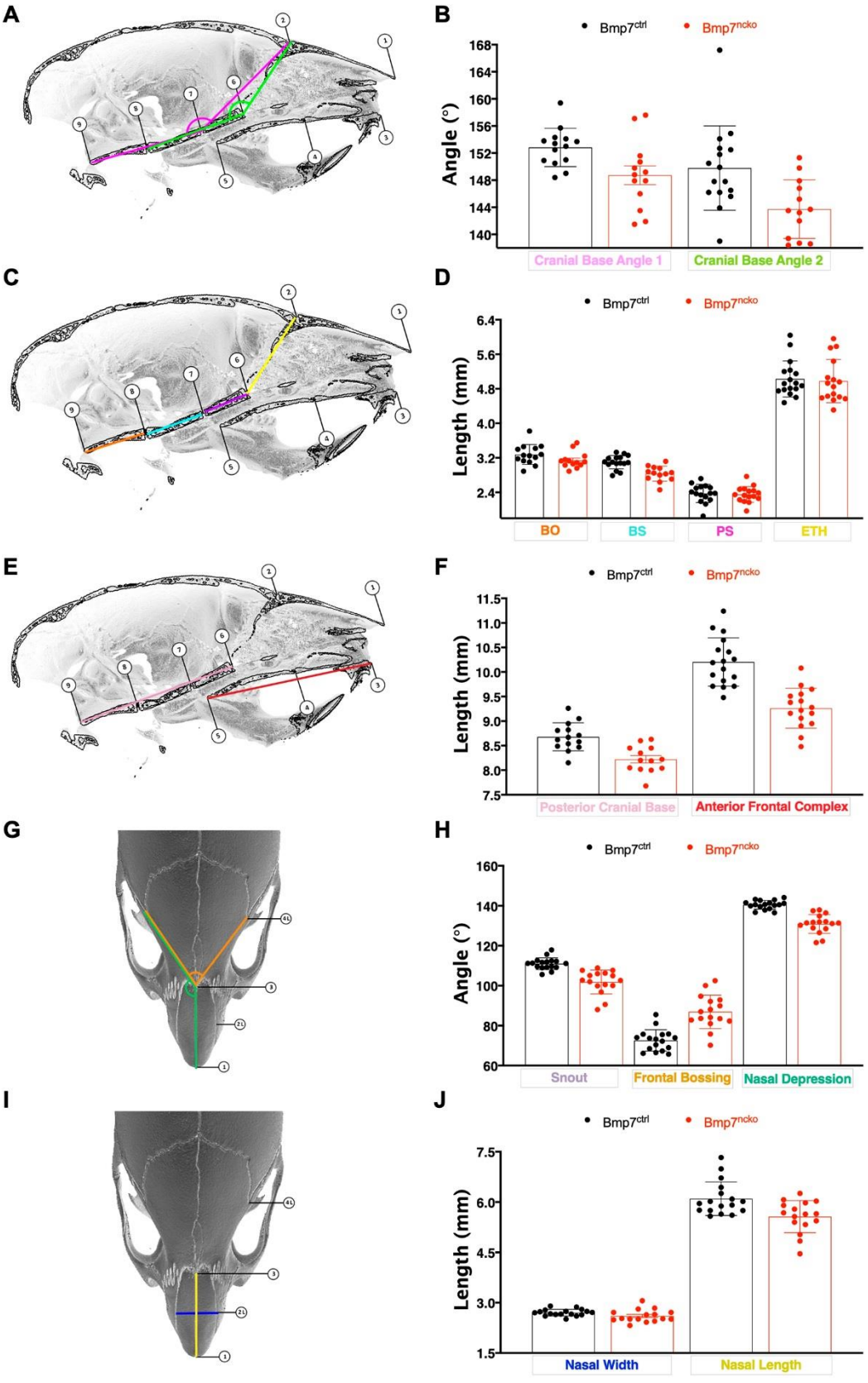

Figure 2. Craniofacial growth defects contributing to midfacial hypoplasia in 1-month Bmp7^{ncko} mice. The angle (A-B) and lengths (C-D) of the individual components forming the cranial base were measured using landmarks placed on mid-sagittal cross-sections of the mouse skulls. **(A)** Angles of cranial base 1 (pink) (n=27) and cranial base 2 (green) (n=29) demonstrated an acute angled cranial base in Bmp7^{ncko} mice with p values of 0.05, 0.23, respectively **(B)**. **(C)** Landmarks used to measure lengths of BO, BS, PS, ETH depicted in orange, cyan, violet, and yellow, respectively. Measurements indicated a reduction in length of BS in the Bmp7^{ncko} mice **(D)** (bo: n=27, p=0.11. bs: n=29, p<0.001. ps: n=32, p=0.76. eth: n=33, p=0.76). **(E)** Landmarks of the posterior cranial base and anterior frontal complex, depicted in pink and red, respectively. **(F)** Measurements demonstrate a significant decrease in both posterior cranial base (n=27, p<0.001) and anterior frontal complex (n=33, p<0.001). Angles of snout **(E)**, frontal bossing **(G)**, and nasal depression **(G)**, depicted in purple, orange, and green respectively. Bmp7^{ncko} mice demonstrate more acute snout angle, increased frontal bossing and more acute angle of nasal depression (n=33, p<0.001) **(H)**. Lengths of nasal bone width and length, depicted in panel **(I)** in blue and yellow, respectively. Measurements of nasal width and length **(J)** suggest that the mutant mice have a decreased nasal bone length (n=33, p<0.05) with no changes to nasal width (n=33, p=0.07). BO: basioccipital length; BS: basisphenoid length; PS: presphenoid length; ETH: ethmoid length. * indicates p<0.05, ** indicates p<0.001. Anatomical description of the landmarks in Fig. S1.

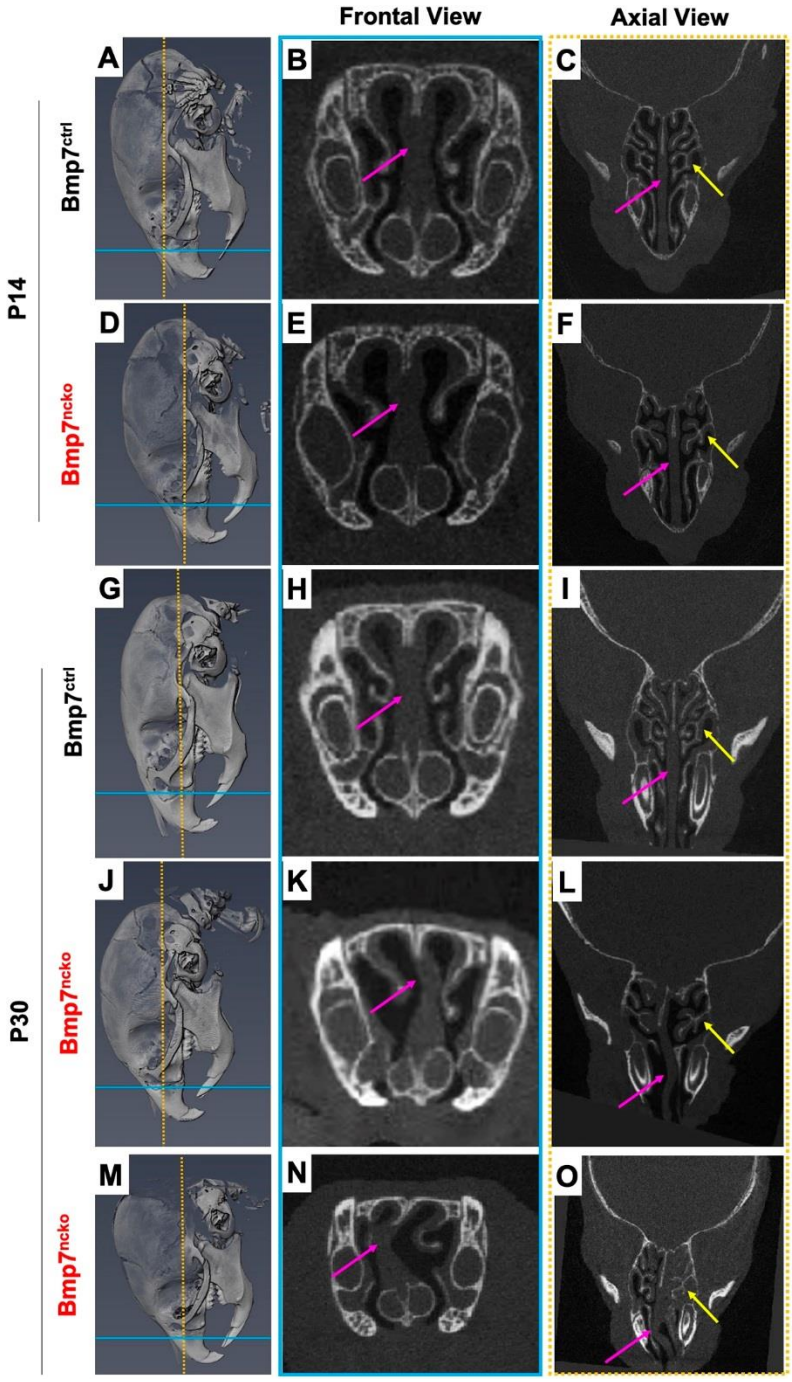

Figure 3. Bmp7^{ncko} mice present with nasal septum deviation and turbinate dysfunction. Micro-computed tomography (µCT) representation of frontal (blue line) and axial planes (orange dotted line) used to characterize nasal septum and turbinate abnormality in 2 week (P14) **(A,D)** and 1-month old mice (P30) **(G, J, M)**. At P14, mice present no structural

differences to the nasal septum (pink arrow) in the control **(B-C)** and mutant **(E-F)** mice under both views. However, abnormal turbinate branching and swelling of mucosa surrounding the turbinates (yellow arrow) was already observed in the mutant mice at 2 weeks **(F)**. At P30, all mutant mice present with nasal septum deviation in both frontal **(K-L)** and axial **(N-O)** views in comparison to the control mice **(H-I)**. However, the degree of nasal septum deviation varies between each mutant **(K vs. N)**. Similarly, turbinate branching dysfunction and swelling of the mucosa persists in the mutant mice **(L-O)** at P30 as well. Frontal views of the nasal cavity are outlined in blue and axial views in orange. n=3/age/genotype.

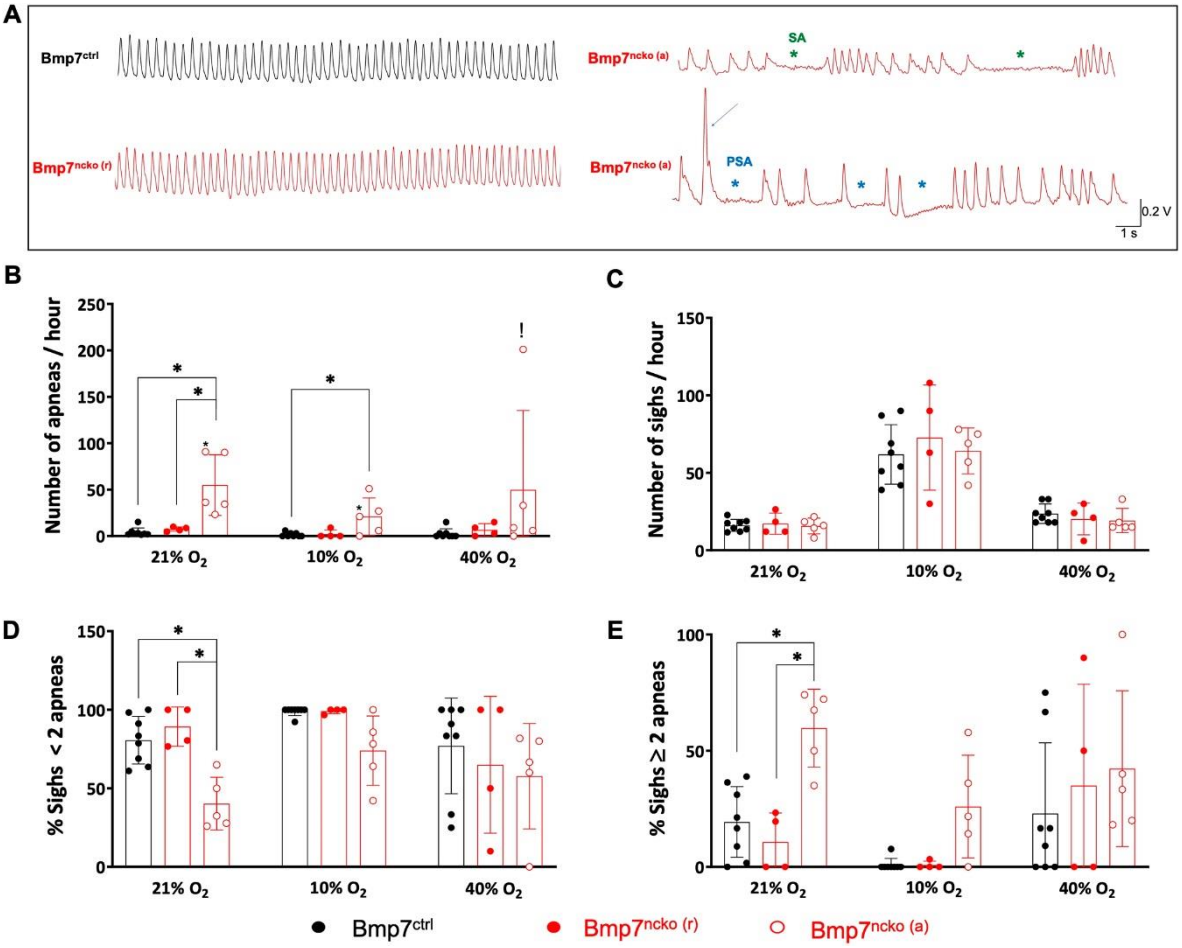

Figure 4. Spontaneous Apnea, Sigh and Post-sigh Apnea during normoxia, hypoxia and hyperoxia in Bmp7^{ctrl}, Bmp7$^{ncko\ (r)}$ and Bmp7$^{ncko\ (a)}$ mice. (A) Representative traces showing normal breathing pattern in Bmp7^{ctrl} (black trace) and Bmp7$^{ncko\ (r)}$ mice; breathing pattern with spontaneous apneas (SA) (green asterisks) in Bmp7$^{Ncko\ (a)}$ mice, and sigh (blue arrow) followed by 3 apneas (blue asterisks). Number of apneas/hour **(B)** and number of sighs/hour **(C)** in the three experimental groups during normoxia (21% O_2), hypoxia (10% O_2) and hyperoxia (40% O_2). Percentage (%) of sighs with < 2 apneas **(D)** and % of sighs with ≥ 2 apneas **(E)** in the three experimental groups during normoxia (21% O_2), hypoxia (10% O_2) and hyperoxia (40% O_2). *Means statistical difference between groups (*$p < 0.05$). $^{!}$ Means outlier. Bmp7$^{ncko\ (r)}$ is used for mutant mice with no changes to regular breathing. Bmp7$^{ncko\ (a)}$ is used to denote Bmp7^{ncko} mice with SA.

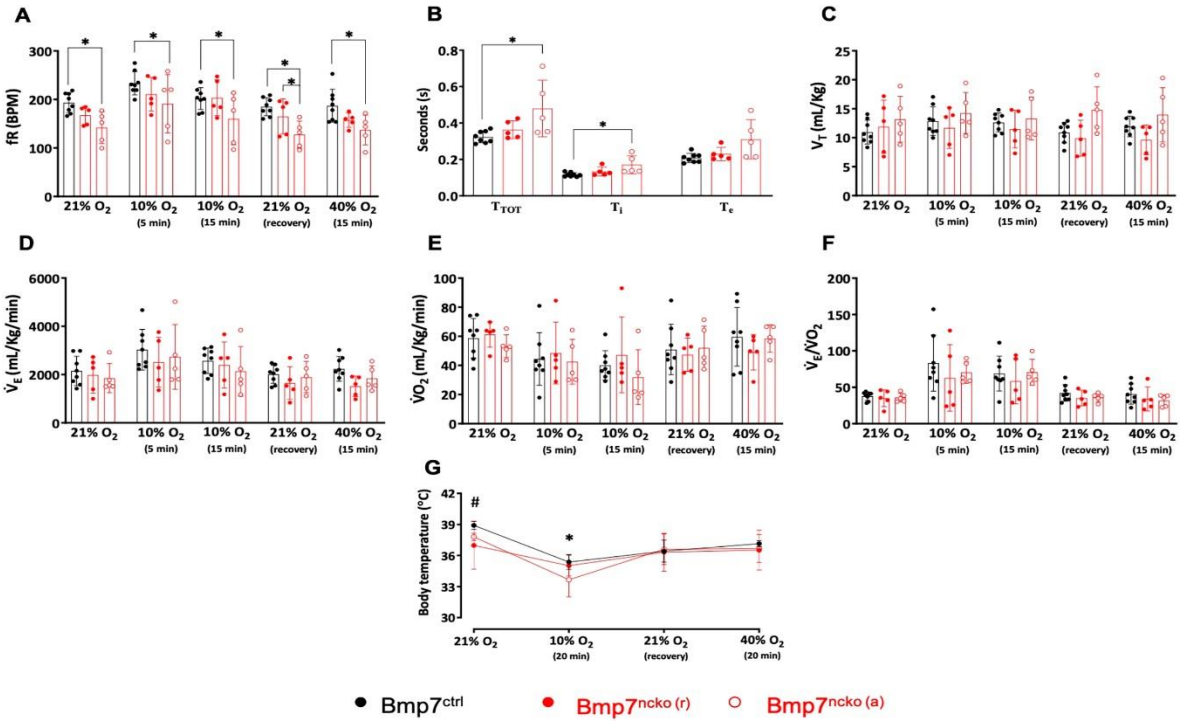

Figure 5. Respiratory and metabolic patterns during normoxia, hypoxia and hyperoxia in Bmp7^{ctrl}, Bmp7$^{ncko\ (r)}$ and Bmp7$^{ncko\ (a)}$ mice. (A) Respiratory frequency (fR) in the three experimental groups during normoxia (21% O_2), 5 and 15 min of hypoxia (10% O_2), recovery to baseline conditions (21% O_2) and 15 min of hyperoxia (40% O_2). **(B)** Breath cycle duration (T_{TOT}), Inspiratory time (T_i) and Expiratory time (T_e) during normoxia in the three experimental groups. **(C-F)** Tidal volume (V_T), Minute Ventilation ($\dot{V}_E$), O_2 consumption ($\dot{V}O_2$), Air convection requirements ($\dot{V}_E$ /$\dot{V}O_2$) in the three experimental groups during normoxia (21% O_2), 5 and 15 min of hypoxia (10% O_2), recovery to baseline conditions (21% O_2) and 15 min of hyperoxia (40% O_2). **(G)** Body temperature (Tb) in the three experimental groups during normoxia (21% O_2), 20 min of hypoxia (10% O_2), recovery to baseline conditions (21% O_2) and 20 min of hyperoxia (40% O2). *Indicates statistical difference between groups (*$p < 0.05$). In the Tb graph, *Indicates statistical difference between Bmp7^{ctrl} and Bmp7$^{ncko\ (a)}$ mice; #Indicates statistical difference between Bmp7^{ctrl} and Bmp7$^{ncko\ (r)}$ mice. Bmp7$^{ncko\ (r)}$ is used for mutant mice with no changes to regular breathing. Bmp7$^{ncko\ (a)}$ is used to denote Bmp7^{ncko} mice with apneas. Eight control mice and 10 Bmp7^{ncko} mice were used in the study.

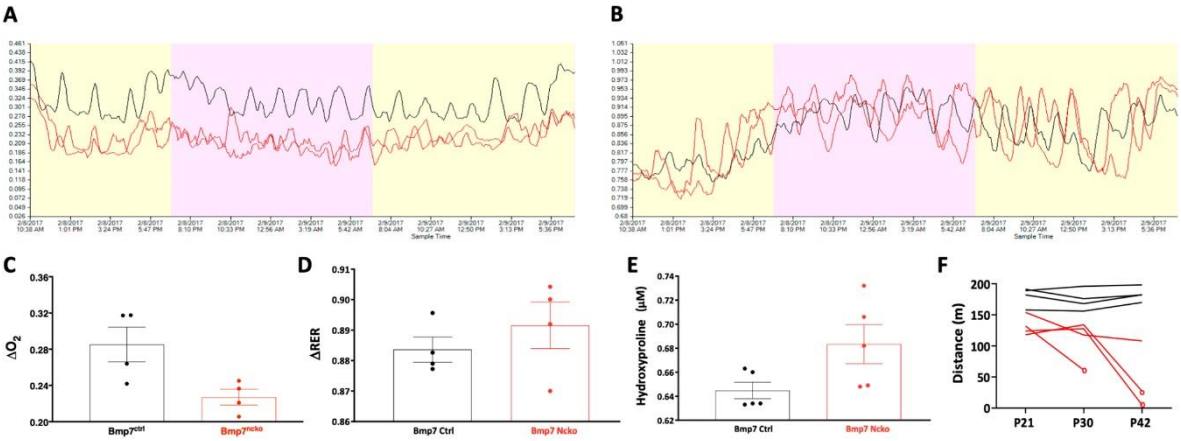

Figure 6. Oxygen consumption is reduced in the Bmp7^{ncko} mice. 1-month old Bmp7^{ctrl} and Bmp7^{ncko} mice were measured in the Comprehensive Lab Monitoring System (CLAMS) chamber for oxygen consumption and respiratory exchange. **(A)** Representative trace of delta oxygen consumption plotted against time for one control (black) and two Bmp7^{ncko} mice (red) demonstrated a reduction in oxygen consumption **(C)** (n=4, p<0.05). **(B)** Representative trace of respiratory exchange ratio (RER) plotted against time for one control (black) and two Bmp7^{ncko} mice (red) demonstrated no significant changes **(D)** (n=4, p=0.39). **(E)** Metabolite analysis of blood serum collected from Bmp7^{ctrl} and Bmp7^{ncko} mice demonstrated a significant upregulation in Hydroxyproline concentration in the mutant mice (n=5, p<0.05) **(F)** Exhaustion treadmill test on Bmp7^{ctrl} and Bmp7^{ncko} mice revealed a reduction in physical activity in the mutant mice (red) as mice age. P21: post-natal day 21; P30: post-natal day 30; P42: post-natal day 42. Circle denotes mutant mice which became severe and had to be euthanized. * indicates p<0.05.

Table

Table 1: Examples of rodent models of airway obstruction and midfacial abnormalities.

Model name	Midfacial abnormality	Hypoxia	Airway obstruction	Respiratory disturbances	References
Mechanical obstruction models					
Tracheal narrowing			x		(Tarasiuk and Segev, 2018)
Tracheal balloon		x	x	x	(Schoorlemmer et al., 2011)
Tracheostomy		x	x	x	(Farré et al., 2018)
Tracheal cannula			x		(Tarasiuk et al., 1991)
Environmental models					
Nasal mask		x	x	x	(Almendros et al., 2011)
Intermittent hypoxia box		x			(Fletcher et al., 1992; Gozal et al., 2001)
Head/body chamber setup		x	x		(Farré et al., 2003)
Long Term Intermittent Hypoxia		x		x	(Veasey, 2009)
Craniofacial genetic models					
Crouzon Syndrome mouse	x				(Perlyn et al., 2006)
Fetal Alcohol Syndrome mouse	x				(Hong and Krauss, 2012)
Osterix-*Cre* transgenic mouse	x				(Huang and Olsen, 2015)
Achondroplasia mouse model	x				(Wang et al., 1999)
$Bmp7^{ncko}$ mouse model	x	(x)	x	x	
SDB genetic models					
Diet Induced Obese (DIO) mouse			x	x	(Berger et al., 2019)
Zucker hooded rat			x		(Iida et al., 1996)
Koletsky rat			x		(Ishizuka et al., 1998; Takaya et al., 1996)
New Zealand obese mouse			x		(Brennick et al., 2009; O'Donnell et al., 2000)
Orexin knock-out mouse				x	(Chemelli et al., 1999; Diniz Behn et al., 2010)

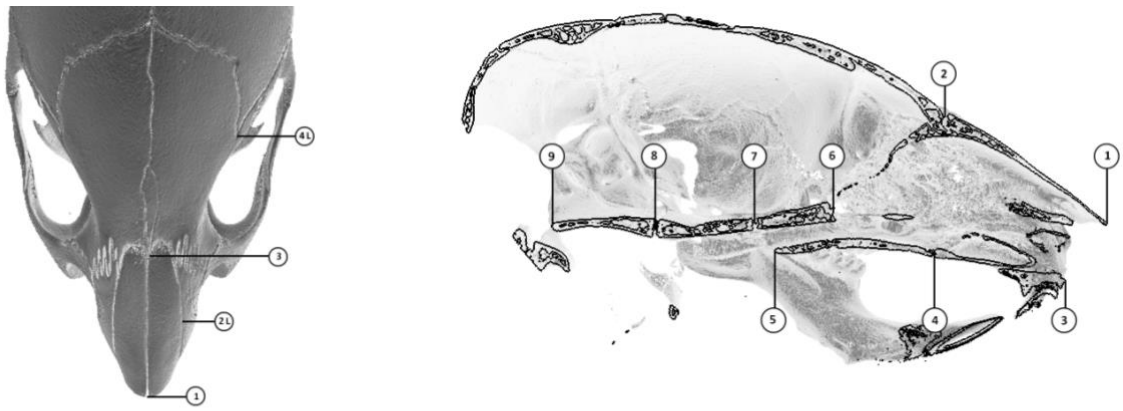

Superior Landmarks

1) Nasale (rostral intersection of nasal bones)
2) Nasion (caudal intersection of nasal bones)
3) External margin of nasal bones (left and right)
4) Frontal-temporal-parietal junction (left and right)

Mid-sagittal Landmarks

1) Nasale (rostral tip of nasal bone)
2) Nasion (intersection of frontal and nasal bone)
3) Anterior-most point of alveolar bone of upper incisor
4) Intersection of maxilla and pre-maxilla
5) Caudal-most point of palatine bone
6) Rostral pre-sphenoid bone
7) Ventral-most point of ISS
8) Ventral-most point of SOS
9) Caudal-most point of basi-occopital bone

Fig. S1. Diagram of morphometric landmarks and measurements used to characterize craniofacial growth, or lack thereof, in Bmp7^{ctrl} and Bmp7^{ncko} mice. (left panel): superior view of the skull. (right panel): mid-sagittal view of the skull.

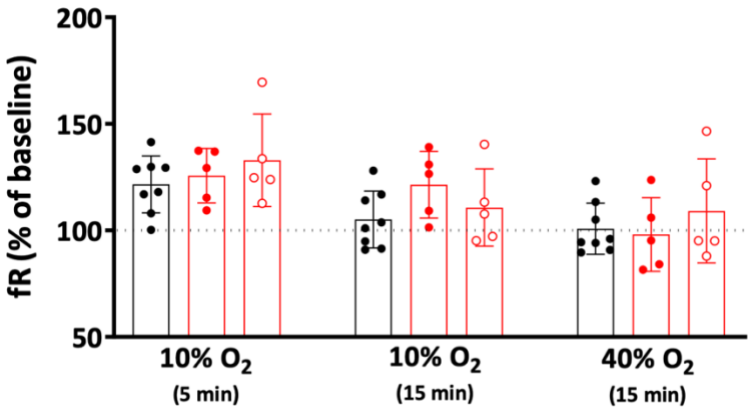

Fig. S2. Respiratory pattern during normoxia in 2-week-old Bmp7^{ctrl} and Bmp7^{ncko} mice. (A) Respiratory frequency (fR). **(B)** Breath cycle duration (TTOT), Inspiratory time (Ti) and Expiratory time (Te). **(C)** Number of apneas/hour. **(D)** Number of sighs/hour. **(E)** Percentage (%) of post sigh apneas (PSA) / total number of sighs with < 2 PSA or ≥ 2 PSA apneas. There was no statistical difference between the groups ($p > 0.05$).

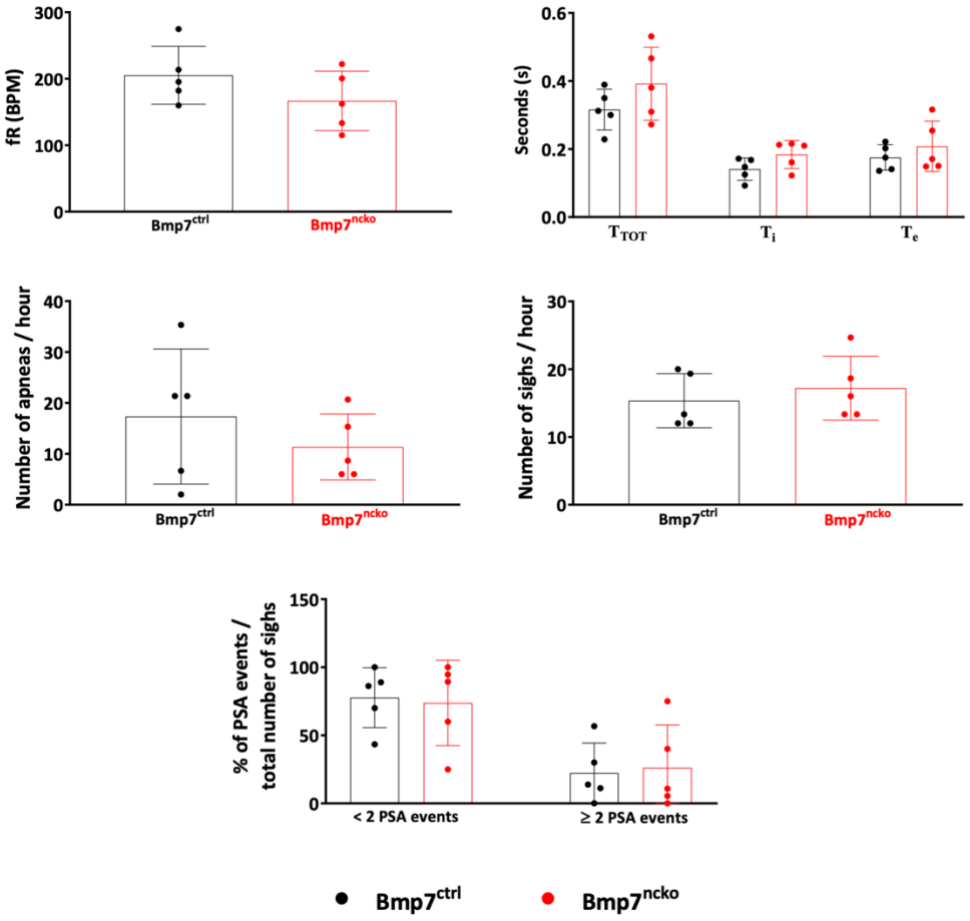

Fig. S3. Respiratory frequency (fR) during hypoxia and hyperoxia exposures. Absolute values from figure 5A shown as percentage (%) of baseline values during 5 and 15 min of hypoxia (10% O2) and 15 min of hyperoxia (40% O2), in $Bmp7^{ctrl}$, $Bmp7^{ncko\ (r)}$ and $Bmp7^{ncko\ (a)}$ mice.

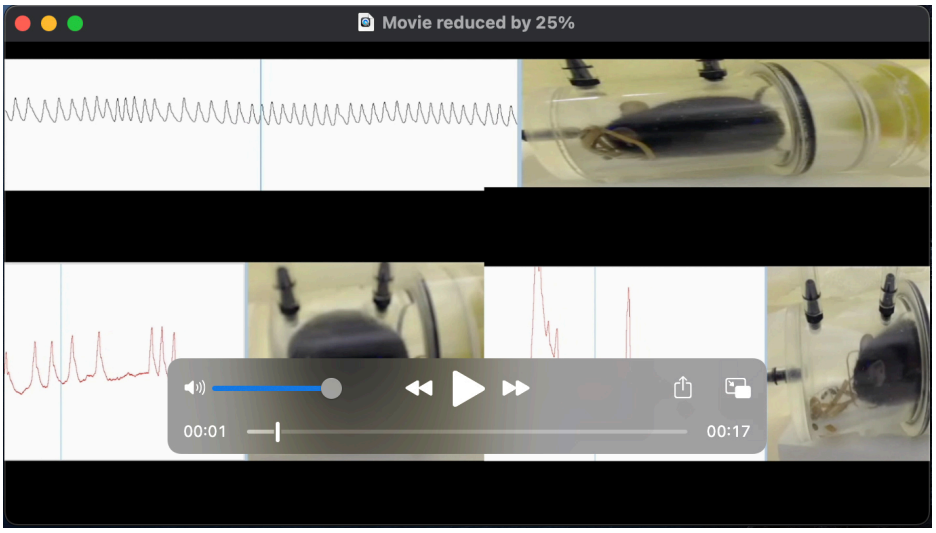

Movie 1. Video representation of Bmp7^{ncko} mice experiencing apneas. Bmp7^{ncko} mice experience spontaneous apnea events Mice were placed in plethysmography chambers and video of the mutant mouse behaviour during baseline measurements was recorded.

Movie 2. Video representation of Bmp7^{ncko} mice demonstrating lethargy. Bmp7^{ctrl} (top panel) and Bmp7^{ncko} (bottom panel) mice were placed on the treadmill for 5 mins after acclimatization to run. The Bmp7^{ctrl} mice demonstrated no signs of inactivity and rest, however the Bmp7^{ncko} mice demonstrate short period of running followed by long periods of rest.

Table S1. Two-tailed independent t-test statistical comparison of control and mutant morphometric data to accompany Figure 1. P14: 2-week-old mice; P21: 3-week-old mice; P30: 1-month-old mice. n=3 for each age group per genotype.

	Age	Degrees of freedom	T statistic	p-value
Facial length				
	P14	3	1.553238	0.218187
**	P21	4	12.44201	0.00024
*	P30	4	7.073297	0.002108
Snout angle				
	P14	2	-0.51867	0.655675
	P21	2	1.393439	0.298145
	P30	4	-1.83126	0.141021
Frontal bossing				
	P14	3	-1.97315	0.143007
	P21	2	-2.56254	0.12448
	P30	3	2.238238	0.111143
Nasal depression				
	P14	4	0.583792	0.590695
	P21	2	2.566908	0.124132
	P30	3	-0.95634	0.409451
Nasal bone width				
	P14	2	-2.77746	0.108867
	P21	4	0.518786	0.631289
	P30	2	0.243733	0.830158
Nasal bone length				
	P14	4	2.003438	0.115662
	P21	3	2.057673	0.13179
	P30	3	-0.04358	0.96798

Table S2. Two-tailed independent t-test statistical results to accompany Figure 2 morphometric data from 1 month old mice. * indicates p<0.05; ** indicates p<0.001. n=3 for each age group per genotype.

	Measurement	Degrees of freedom	T statistic	p-value
*	cranial base angle 1	19	2.607641	0.017301
	cranial base angle 2	23	1.225689	0.232719
	basioccipital length	25	1.669665	0.107462
**	basisphenoid length	25	5.914634	3.58E-06
	presphenoid length	29	0.313573	0.75609
	ethmoid length	29	0.311218	0.757861
**	posterior cranial base length	25	4.27551	0.000244
**	facial length	31	6.013647	1.18E-06
**	snout angle	22	5.541883	1.43E-05
	cranium maxilla angle	23	0.610879	0.54727
**	frontal bossing	25	-5.79575	4.84E-06
**	nasal depression	21	7.335938	3.21E-07
	nasal bone width	22	1.879617	0.07347
*	nasal bone length	31	3.12455	0.003847

Table S3. $Bmp7^{ncko}$ mice showed no changes to cranial base angles and lengths prior to nasal septum deviation. P14: 2-week-old-mice; P21: 3-week-old-mice; n=3 for each age group per genotype.

Measurement	P14 $Bmp7^{ctrl}$	P14 $Bmp7^{ncko}$	p-value	P21 $Bmp7^{ctrl}$	P21 $Bmp7^{ncko}$	p-value
cranial base angle 1	154.93±1.42	151.66±5.99	0.40	150.55±2.71	144.46±6.62	0.13
cranial base angle 2	150.64±2.50	148.18±4.44	0.31	146.48±4.46	143.64±5.20	0.42
basioccipital length	2.89±0.33	2.758±0.15	0.44	3.32±0.71	2.93±0.29	0.29
basisphenoid length	2.712±0.20	2.468±0.19	0.086	2.67±0.31	2.69±0.37	0.92
presphenoid length	2.14±0.12	2.04±0.19	0.35	2.21±0.17	2.14±0.13	0.50
ethmoid length	4.36±0.28	4.5±0.37	0.53	4.95±0.27	4.88±0.22	0.72
posterior cranial base length	8.03±0.26	7.75±0.23	0.11	8.09±0.75	7.67±0.23	0.27

Table S4. Intraclass correlation (ICC) assessment to address intrarater reliability. Three P30 mice of each genotype were landmarked and measured in triplicate by a single rater.

		confidence interval	
mouse ID	ICC	lower	upper
C324	0.999524	0.998854	0.999833
C325	0.999798	0.999513	0.999929
C327	0.999274	0.998253	0.999746
C531	0.996789	0.992222	0.998877
C586	0.997853	0.994838	0.999247
C600	0.998306	0.995721	0.999416
K3308	0.998042	0.995252	0.999315
K3309	0.998773	0.997022	0.999571